.

COMPUTATIONAL MECHANICS - THEORY AND PRACTICE
K.M. Mathisen, T. Kvamsdal and K.M. Okstad (Eds.)

A TEMPLATE TUTORIAL

Carlos A. Felippa

Department of Aerospace Engineering Sciences
and Center for Aerospace Structures
University of Colorado, CB 429
Boulder, CO 80309-0429, USA
Email: carlos.felippa@colorado.edu
Web page: http://titan.colorado.edu/Felippa.d/FelippaHome.d/Home.html

Dedicated to Pål Bergan on his 60th birthday

Abstract. This article has a dual theme: historical and educational. It is a tutorial on finite element templates for two-dimensional structural problems. The exposition is aimed at readers with introductory level knowledge of finite element methods. It focuses on the four-node plane stress element of flat rectangular geometry, called the "rectangular panel" for brevity. This is one of the two oldest continuum structural elements. On the other hand the concept of finite element templates is a recent development, which had as key source the 1984–87 collaboration between Pål Bergan and the writer on the Free Formulation. Interweaving the old and the new throws historical perspective into the evolution of finite element methods. Templates provide a framework in which diverse element formulations can be fitted, compared and traced back to the sources. On the technical side templates facilitate the unified implementation of element families, as well as the construction of custom elements. To illustrate customization power beyond the rectangle, the Appendix presents the construction of a four-noded bending-optimal trapezoid. This model sidesteps MacNeal's limitation theorem in that it passes the patch test for any geometry while staying bending-optimal along one direction and retaining full rank.

Key words: finite elements, history, templates, families, clones, quadrilateral membrane, Free Formulation, patch test

1 INTRODUCTION

This article interweaves historical and educational themes with the presentation of a new methodology for finite element development. It is expository in nature, and focuses on "FEM by its history." It gently exposes the reader to the concept of templates, and explains why they emerge naturally from historical evolution. Much of the material is tutorial in nature, with some extracted from a FEM course offered by the writer.

Templates are parametrized algebraic forms that provide a continuum of consistent and stable finite element models of a given type and node/freedom configuration. Template instances produced by setting values to free parameters furnish specific elements. If the template embodies all possible consistent and stable elements of a given type and configuration, it is called *universal*.

Befitting the tutorial aim, the main body of this article focuses on the simplest two-dimensional element that possesses a nontrivial template: the four-node plane stress element of flat rectangular geometry. [The three-node linear triangle is simpler but its template is trivial.] This is called the *rectangular panel* for brevity.

The rectangular panel is interesting from both historical and instructional viewpoints because:

1. It is one of the two oldest continuum finite elements, the other being the linear triangle.[1]
2. Along with its plane strain and axisymmetric cousins, it is the configuration treated by most new methods since the birth of finite elements. As such it represents an *in-vivo* specimen of FEM evolution over the past 50 years.
3. It is amenable to complete analytical development, even for anisotropic material behavior. This makes the element particularly suitable for homework and project assignments.
4. Analytical forms make the concept of signatures and clones highly visible to students.

The paper is organized as follows. Section 2 is a brief outline of element formulation approaches used from 1950 to date. Section 3 introduces the focus problem. Sections 4–6 follow up on the historical theme by presenting stress, strain and displacement-based models for the rectangular panel.

The concept of template is introduced in Section 7 by calling attention to a common structure that lurks behind the stiffness expressions of stress, strain and displacement models. Template terminology follows as consequence: families, signatures, instances and clones. The role of higher order patch tests in optimality is illustrated in Sections 8 and 9. SRI schemes are presented in Section 10 from the template standpoint to show that this approach naturally leads to correct splittings of the elasticity law. The concept of element families is illustrated in Section 11 using stress hybrid and displacement bubbles as examples. These clearly illuminate the futility of the "enrichment" approaches popular in the late sixties. Section 12 provides numerical examples and Section 13 offers conclusions.

The Appendix presents the construction of a four-noded bending-optimal trapezoid. Although this illustrates the customization power of templates beyond rectangles, the more advanced mathematical tools in use behind the scenes can make the results look like black magic to beginners. The optimal trapezoid partly circumvents MacNeal's limitation theorem[2] in that it passes the patch test for arbitrary geometry and material and is bending optimal along one direction, while retaining a bounded condition number and thus fulfilling the inf-sup condition.

A sequel to this article[3] covers the generalization to an a optimal quadrilateral of arbitrary shape. The algebraic manipulations are beyond the power of any human to work out by hand over a lifetime, so in retrospect it is not surprising that this model has not been discovered sooner. Fortunately the symbolic work falls, although barely, within the grasp of computer algebra systems on a PC. The final results are surprisingly simple and elegant, even for arbitrary anisotropic material. The construction finishes a quest that has preoccupied FEM investigators over several decades.

2 HISTORICAL SKETCH

This section summarizes the history of structural finite elements since 1950 to date. It functions as a hub for dispersed historical references. Readers uninterested in these aspects should proceed directly to Section 3. For exposition convenience, structural "finitelementology" may be divided into four generations that span 10 to 15 years each. There are no sharp intergenerational breaks, but noticeable changes of emphasis. The ensuing outline

does not cover the conjoint evolution of Matrix Structural Analysis into the Direct Stiffness Method from 1934 through 1970. This was the subject of a separate essay.[4]

2.1 G1: The Pioneers

The 1956 paper by Turner, Clough, Martin and Topp,[1] henceforth abbreviated to TCMT, is recognized as the start of the current FEM, as used in the overwhelming majority of commercial codes. Along with Argyris' serial[5] they prototype the first generation, which spans 1950 through 1962. A panoramic picture of this period is available in two textbooks.[6,7] Przemieniecki's text is still reprinted by Dover. The survey by Gallagher[8] was influential but is now difficult to access.

The pioneers were structural engineers, schooled in classical mechanics. They followed a century of tradition in regarding structural elements as a device to transmit forces. This "element as force transducer" was the standard view in pre-computer structural analysis. It explains the use of flux assumptions to derive stiffness equations. Element developers worked in, or interacted closely with, the aircraft industry. [One reason is that only large aerospace companies were then able to afford mainframe computers.] Accordingly they focused on thin structures built up with bars, ribs, spars, stiffeners and panels. Although the Classical Force method dominated stress analysis during the fifties,[4] stiffness methods were kept alive by use in dynamics and vibration.

2.2 G2: The Golden Age

The next period spans the golden age of FEM: 1962–1972. This is the "variational generation." Melosh[9] showed that conforming displacement models are a form of Rayleigh-Ritz based on the minimum potential energy principle. This influential paper marks the confluence of three lines of research: Argyris' dual formulation of energy methods,[5] the Direct Stiffness Method (DSM) of Turner,[10–12] and early ideas of interelement compatibility as basis for error bounding and convergence.[13,14] G1 workers thought of finite elements as idealizations of structural components. From 1962 onward a two-step interpretation emerges: discrete elements approximate continuum models, which in turn approximate real structures.

By the early 1960s FEM begins to expand into Civil Engineering through Clough's Boeing-Berkeley connection[15] and had been named.[16,17] Reading Fraeijs de Veubeke's celebrated article[18] side by side with TCMT [1] one can sense the ongoing change in perspective opened up by the variational framework. The first book devoted to FEM appears in 1967.[19] Applications to nonstructural problems start by 1965.[20]

From 1962 onwards the displacement formulation dominates. This was given a big boost by the invention of the isoparametric formulation and related tools (numerical integration, fitted coordinates, shape functions, patch test) by Irons and coworkers.[21–25] Low order displacement models often exhibit disappointing performance. Thus there was a frenzy to develop higher order elements. Other variational formulations, notably hybrids,[26–29] mixed[30,31] and equilibrium models[18] emerged. G2 can be viewed as closed by the monograph of Strang and Fix,[32] the first book to focus on the mathematical foundations.

2.3 G3: Consolidation

The post-Vietnam economic doldrums are mirrored during this post-1972 period. Gone is the youthful exuberance of the golden age. This is consolidation time. Substantial effort is put into improving the stock of G2 displacement elements by tools initially labeled "variational crimes" by Strang,[33] but later justified. Textbooks by Hughes[34] and Bathe[35] reflect the technology of this period. Hybrid and mixed formulations record steady progress.[36] Assumed strain formulations appear.[37] A booming activity in error estimation and mesh adaptivity is fostered by better understanding of the mathematical foundations.[38]

Commercial FEM codes gradually gain importance. They provide a reality check on what works in the real world and what doesn't. By the mid-1980s there was gathering evidence that complex and high order elements were commercial flops. Exotic gadgetry interweaved amidst millions of lines of code easily breaks down in new releases. Complexity is particularly dangerous in nonlinear and dynamic analyses conducted by novice users. A trend back toward simplicity starts.[39,40]

2.4 G4: Back to Basics

The fourth generation begins by the early 1980s. More approaches come on the scene, notably the Free Formulation of Bergan,[41,42] which is further discussed below, orthogonal hourglass control,[43] Assumed Natural Strain methods,[44–47] stress hybrid models in natural coordinates,[48–50] as well as variants and derivatives of those approaches: ANDES,[51,52] EAS[53,54] and others. Although technically diverse the G4 approaches share two common objectives:

(i) Elements must fit into DSM-based programs since that includes the vast majority of production codes, commercial or otherwise.

(ii) Elements are kept simple but should provide answers of engineering accuracy with relatively coarse meshes. These were collectively labeled "high performance elements" in 1989.[55]

"Things are always at their best in the beginning," said Pascal. Indeed. By now FEM looks like an aggregate of largely disconnected methods and recipes. Sections 4-6 look at three disparate components of this edifice to anticipate the subsequent exhibition of common features by templates.

2.5 From the Free Formulation to Templates

In the early 1970s Pål Bergan — then a Professor at NTH-Trondheim — and L. Hanssen published a paper[56] in MAFELAP II, where a different approach to finite elements was advocated. The concept is well outlined in the Introduction of that paper:

> "An important observation is that each element is, in fact, only represented by the numbers in its stiffness matrix during the analysis of the assembled system. The origin of these stiffness coefficients is unimportant to this part of the solution process ... The present approach is in a sense the opposite of that normally used in that the starting point is a generally formulated convergence condition and from there the stiffness matrix is derived ... The patch test is particularly attractive [as such a condition] for the present investigation in that it is a direct test on the element stiffness matrix and requires no prior knowledge of interpolation functions, variational principles, etc."

This statement sets out what may be called the *direct algebraic approach* to finite elements: the element stiffness is to be derived directly from consistency conditions — provided by the Individual Element Test of Bergan and Hanssen[56,57] — plus stability and accuracy considerations to determine algebraic redundancies if any.

This ambitious goal proved initially elusive because the direct algebraic construction of the stiffness matrix of most multidimensional elements becomes effectively a problem in constrained optimization. In the *symbolic form* necessitated by element design, such problem is much harder to tackle than the conventional element construction methods. A constructive step was provided by the Free Formulation, which emerged over the next decade.[42] The foregoing difficulties were addressed using divide and conquer. The stiffness is decomposed into a basic part that takes care of consistency and mixability, and a higher order (HO) part that takes care of stability (rank sufficiency) and accuracy. Orthogonality conditions enforced between the two parts avoid pollution of the basic element response by the higher order component.

The writer's acquaintance with the FF began in 1984, while Pål Bergan was spending a 9-month sabbatical at Stanford. At the time the writer was in the staff of the Applied

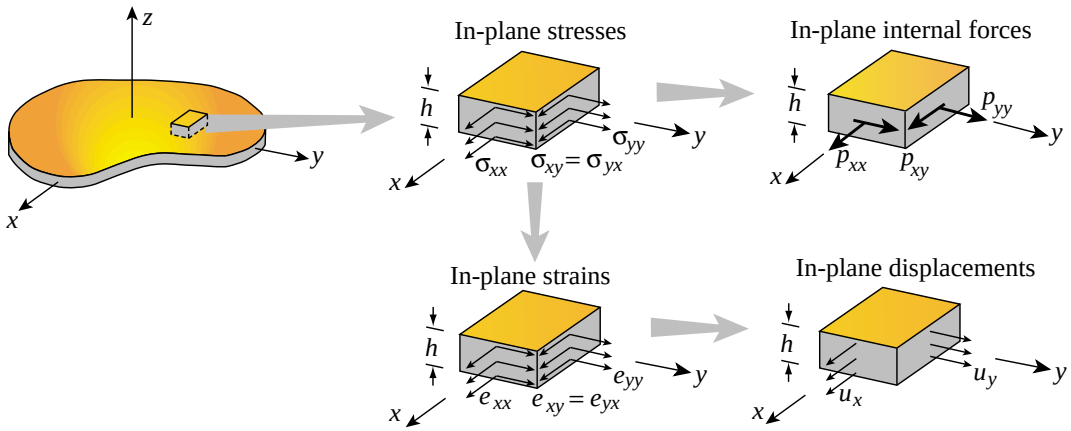

Figure 1. A thin plate in plane stress, illustrating notation.

Mechanics Laboratory of Lockheed Palo Alto Research Laboratories (LPARL, located in the Stanford Industrial Park), involved in gruelling software development supporting the Trident II system and underwater shock analysis codes. Our collaboration, supported by the LPARL Independent Research program, was the first element-related project undertaken by the writer since Berkeley days. It was a welcome respite from the software grind. It resulted in the first rank-sufficient triangular membrane element with drilling freedoms that passed the IET. Tom Hughes kindly speeded up publication.[58]

The move to the University of Colorado in 1986 allowed the writer to pursue further these ideas within an academic environment. In the FF the HO stiffness was based on a displacement formulation, whereas the basic stiffness is method independent. Other techniques were tried for the HO stiffness. Particularly successful was a modification of the Assumed Natural Strain (ANS) method of Park and Stanley.[46,47] In this variant only the deviatoric part of the assumed strains was carried forward, and the ANDES method emerged.[51,52] Gradually the realization dawned that *all consistent and rank sufficient elements*, no matter how they are derived, must fit an algebraic form with free parameters, baptized as *template*. This "template as umbrella" concept emerged by 1990. It has since developed by fits and starts. The current status of the subject is summarized in Section 13.

3 PROBLEM DESCRIPTION

3.1 Governing Equations

Consider the thin homogeneous plate in plane stress shown in Figure 1. The inplane displacements are $\{u_x, u_y\}$, the associated strains are $\{e_{xx}, e_{yy}, e_{xy}\}$ and the inplane (membrane) stresses are $\{\sigma_{xx}, \sigma_{yy}, \sigma_{xy}\}$. Prescribed inplane body forces are $\{b_x, b_y\}$, but they will be set to zero in derivations of equilibrium elements. Prescribed displacements and surface tractions are denoted by $\{\hat{u}_x, \hat{u}_y\}$ and $\{\hat{t}_x, \hat{t}_y\}$ respectively. All fields are considered uniform through the thickness h. The governing plane-stress elasticity equations are

$$\begin{bmatrix} e_{xx} \\ e_{yy} \\ 2e_{xy} \end{bmatrix} = \begin{bmatrix} \partial/\partial x & 0 \\ 0 & \partial/\partial y \\ \partial/\partial y & \partial/\partial x \end{bmatrix} \begin{bmatrix} u_x \\ u_y \end{bmatrix}, \qquad \begin{bmatrix} \sigma_{xx} \\ \sigma_{yy} \\ \sigma_{xy} \end{bmatrix} = \begin{bmatrix} E_{11} & E_{12} & E_{13} \\ E_{12} & E_{22} & E_{23} \\ E_{13} & E_{23} & E_{33} \end{bmatrix} \begin{bmatrix} e_{xx} \\ e_{yy} \\ 2e_{xy} \end{bmatrix},$$
$$\begin{bmatrix} \partial/\partial x & 0 & \partial/\partial y \\ 0 & \partial/\partial y & \partial/\partial x \end{bmatrix} \begin{bmatrix} \sigma_{xx} \\ \sigma_{yy} \\ \sigma_{xy} \end{bmatrix} + \begin{bmatrix} b_x \\ b_y \end{bmatrix} = \begin{bmatrix} 0 \\ 0 \end{bmatrix}. \tag{1}$$

The compact matrix version of (1) is

$$\mathbf{e} = \mathbf{D}\mathbf{u}, \qquad \boldsymbol{\sigma} = \mathbf{E}\mathbf{e}, \qquad \mathbf{D}^T\boldsymbol{\sigma} + \mathbf{b} = \mathbf{0}, \tag{2}$$

in which **E** is the plane stress elasticity matrix. Assuming this to be nonsingular, the inverse of $\boldsymbol{\sigma} = \mathbf{E}\mathbf{e}$ is

$$\begin{bmatrix} e_{xx} \\ e_{yy} \\ 2e_{xy} \end{bmatrix} = \begin{bmatrix} C_{11} & C_{12} & C_{13} \\ C_{12} & C_{22} & C_{23} \\ C_{13} & C_{23} & C_{33} \end{bmatrix} \begin{bmatrix} \sigma_{xx} \\ \sigma_{yy} \\ \sigma_{xy} \end{bmatrix}, \quad \text{or} \quad \mathbf{e} = \mathbf{C}\boldsymbol{\sigma}, \tag{3}$$

where $\mathbf{C} = \mathbf{E}^{-1}$ is the matrix of elastic compliances.

3.2 The Rectangular Panel

The focus of this tutorial exposition is the *rectangular panel*. This is depicted in Figure 2. For an individual element the side-aligned local axes are also denoted as $\{x, y\}$ for brevity. The inplane dimensions are a and $b = a/\gamma$, where $\gamma = a/b$ is the aspect ratio. The thickness and elastic properties are constant over the element. The element has 4 corner nodes and 8 external (connective) degrees of freedom. The node displacement and force vectors are configured as

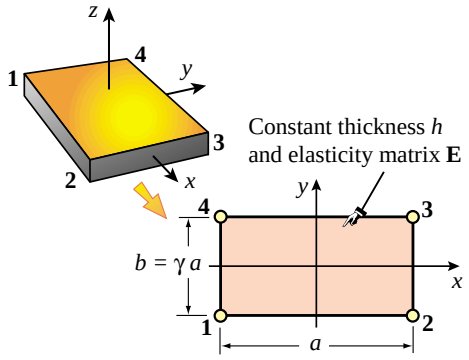

Figure 2. The rectangular panel.

$$\mathbf{u} = [\, u_{x1} \quad u_{y1} \quad u_{x2} \quad u_{y2} \quad u_{x3} \quad u_{y3} \quad u_{x4} \quad u_{y4} \,]^T, \tag{4}$$

$$\mathbf{f} = [\, f_{x1} \quad f_{y1} \quad f_{x2} \quad f_{y2} \quad f_{x3} \quad f_{y3} \quad f_{x4} \quad f_{y4} \,]^T. \tag{5}$$

As noted in the Introduction, most of the FEM formulation methods chronicled in Section 2 have been tried on this configuration as well as its plane strain and axisymmetric cousins. The reason for this popularity is that the rectangular panel is the *simplest multi-dimensional element that can be improved.* [The three-node linear triangle is simpler but cannot be improved.]

In keeping with the expository theme, the next three sections derive the rectangular panel stiffness from stress, strain and displacement assumptions, respectively. Mirroring history, the derivation of stress and strain models follows the matrix-based direct elasticity approach used by the first generation, as summarized in Gallagher's review.[8]

Ironically, the direct derivation from stress modes a la TCMT furnishes optimal or near-optimal elements with little toil, whereas the variationally derived displacement models will need tweaking to become useful.

4 THE STRESS ELEMENT

TCMT[1] is the starting point. In a historical summary Clough[15] remarks that the paper belatedly reports work performed at Boeing's Commercial Airplane Division in 1952–53 (indeed a TCMT footnote states that the material was presented at the 22nd Annual Meeting of IAS, held on January 25–29, 1954.) Besides bars, beams and spars, TCMT presents two plane stress elements for modeling wing cover plates: the three-node triangle and the four-node flat rectangular panel. Quadrilateral panels of arbitrary geometry, not necessarily flat, are constructed as assemblies of four triangles.

Readers perusing that article for the first time have a surprise in store. The stiffness properties of both panel elements are derived from stress assumptions, rather than displacements, as became popular in the second generation. More precisely, simple patterns

of interelement boundary tractions (a.k.a. stress flux modes) that satisfy internal equilibrium are taken as starting point. Twenty years later Fraeijs de Veubeke[59] systematically extended the same idea in a variational setting, to produce what he called diffusive equilibrium elements. These are designed to weakly enforce interelement flux conservation. The comedy continues: mathematicians recently rediscovered flux elements, now renamed as "Discontinuous Galerkin Methods," blessfully unaware of previous work.

The derivation below largely follows Chapter 3 of Gallagher,[8] who presents a step by step procedure for what he calls the "equivalent force" approach. The main extension provided here is allowing for anisotropic material.

4.1 The 5-Parameter Stress Field

Since TCMT the appropriate stress field for the rectangular panel is known to be

$$\sigma_{xx} = \mu_1 + \mu_4 \frac{y}{b}, \quad \sigma_{yy} = \mu_2 + \mu_5 \frac{x}{a}, \quad \sigma_{xy} = \mu_3. \tag{6}$$

The five μ_i are stress-amplitude parameters with dimension of stress. They are collected in the 5-vector

$$\boldsymbol{\mu} = [\,\mu_1 \quad \mu_2 \quad \mu_3 \quad \mu_4 \quad \mu_5\,]^T. \tag{7}$$

The field (6) satisfies the internal equilibrium equations $(1)_3$ under zero body forces. Evaluation over element sides produces the traction patterns of Figure 3, transcribed verbatim from TCMT. Why five? On p. 813: "These load states are seen to represent uniform and linearly varying stresses plus constant shear, along the plate edges. Later it will be seen that the number of load states must be $2n-3$, where n = number of nodes."

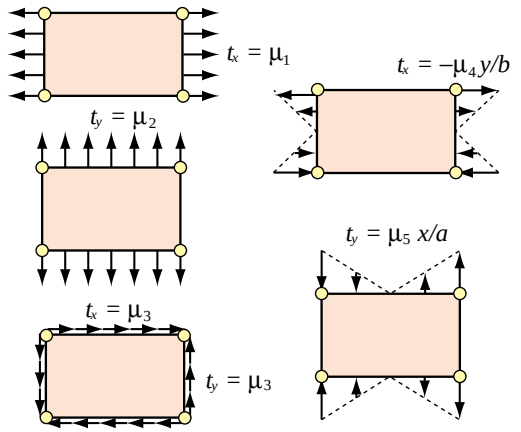

Figure 3. Interelement boundary tractions associated with the stress parameters μ_i in (7). After TCMT, p. 812, in which these five patterns are called "load states."

To establish connection to node displacements, $\boldsymbol{\mu}$ is extended as

$$\boldsymbol{\mu}_+ = [\,\mu_1 \quad \mu_2 \quad \mu_3 \quad \mu_4 \quad \mu_5 \quad \mu_6 \quad \mu_7 \quad \mu_8\,]^T \tag{8}$$

This array contains three dimensionless coefficients: μ_6, μ_7 and μ_8, which define amplitudes of the three element rigid body modes (RBMs):

$$\text{RBM}_1\text{: } u_x{=}\mu_6 a,\ u_y{=}0,\ \text{RBM}_2\text{: } u_x{=}0,\ u_y{=}\mu_7 b,\ \text{RBM}_3\text{: } u_x{=}{-}\mu_8 y,\ u_y{=}\mu_8 x. \tag{9}$$

These modes produce zero stress. The foregoing relations may be recast in matrix form:

$$\boldsymbol{\sigma} = \mathbf{N}\,\boldsymbol{\mu} = \mathbf{N}_+\boldsymbol{\mu}_+, \quad \mathbf{N} = \begin{bmatrix} 1 & 0 & 0 & \frac{y}{b} & 0 \\ 0 & 1 & 0 & 0 & \frac{x}{a} \\ 0 & 0 & 1 & 0 & 0 \end{bmatrix}, \quad \mathbf{N}_+ = \begin{bmatrix} 1 & 0 & 0 & \frac{y}{b} & 0 & 0 & 0 & 0 \\ 0 & 1 & 0 & 0 & \frac{x}{a} & 0 & 0 & 0 \\ 0 & 0 & 1 & 0 & 0 & 0 & 0 & 0 \end{bmatrix}. \tag{10}$$

The boundary traction patterns of Figure 3 are converted to node forces by statics. This yields

$$\mathbf{f} = \mathbf{A}\,\boldsymbol{\mu}, \qquad \mathbf{A}^T = \tfrac{1}{2}h \begin{bmatrix} -b & 0 & b & 0 & b & 0 & -b & 0 \\ 0 & -a & 0 & -a & 0 & a & 0 & a \\ -a & -b & -a & b & a & b & a & -b \\ \frac{1}{6}b & 0 & -\frac{1}{6}b & 0 & \frac{1}{6}b & 0 & -\frac{1}{6}b & 0 \\ 0 & \frac{1}{6}a & 0 & -\frac{1}{6}a & 0 & \frac{1}{6}a & 0 & -\frac{1}{6}a \end{bmatrix}. \tag{11}$$

Matrix **A** is the equilibrium matrix, also known as the leverage matrix in the FEM literature. When restricted to constant stress states (the first three columns of **A**), it is called a force-lumping matrix and denoted by **L** in the Free Formulation of Bergan.[41,42,58,60–65]

4.2 The Generalized Stiffness

Integrating the complementary energy density $\mathcal{U}^* = \frac{1}{2}\boldsymbol{\sigma}^T\mathbf{C}\boldsymbol{\sigma}$ over the element volume V and identifying $U^* = \int_{V^e}\mathcal{U}^*\,dV$ with $\frac{1}{2}\boldsymbol{\mu}^T\mathbf{F}_\mu\boldsymbol{\mu}$ yields the 5×5 flexibility matrix $\mathbf{F}_\mu$ in terms of the stress parameters. Its inverse is the generalized stiffness matrix $\mathbf{S}_\mu = \mathbf{F}_\mu^{-1}$:

$$\mathbf{F}_\mu = V\begin{bmatrix} C_{11} & C_{12} & C_{13} & 0 & 0\\ C_{12} & C_{22} & C_{23} & 0 & 0\\ C_{13} & C_{23} & C_{33} & 0 & 0\\ 0 & 0 & 0 & \frac{1}{12}C_{11} & 0\\ 0 & 0 & 0 & 0 & \frac{1}{12}C_{22}\end{bmatrix},\quad \mathbf{S}_\mu = \frac{1}{V}\begin{bmatrix} E_{11} & E_{12} & E_{13} & 0 & 0\\ E_{12} & E_{22} & E_{23} & 0 & 0\\ E_{13} & E_{23} & E_{33} & 0 & 0\\ 0 & 0 & 0 & 12C_{11}^{-1} & 0\\ 0 & 0 & 0 & 0 & 12C_{22}^{-1}\end{bmatrix}, \tag{12}$$

in which $V = abh$ is the volume of the element.

4.3 The Physical Stiffness

Integration of the slave strain field $\mathbf{e} = \mathbf{E}^{-1}\boldsymbol{\sigma} = \mathbf{C}\mathbf{N}_+\boldsymbol{\mu}_+$ produces the displacement field

$$\begin{aligned} u_x(x,y) &= \mu_6 a + \tfrac{1}{8}\omega_6 + (\mu_1 C_{11}+\mu_2 C_{12}+\mu_3 C_{13})x + (\tfrac{1}{2}(\mu_1 C_{13}+\mu_2 C_{23}+\mu_3 C_{33}) - \mu_8)y\\ &\quad + \tfrac{1}{2}(\mu_5/a)C_{12}x^2 + (\mu_4/b)C_{11}xy + \tfrac{1}{2}\big((\mu_4/b)C_{13} - (\mu_5/a)C_{22}\big)y^2,\\ u_y(x,y) &= \mu_7 b + \tfrac{1}{8}\omega_7 + (\tfrac{1}{2}(\mu_1 C_{13}+\mu_2 C_{23}+\mu_3 C_{33})+\mu_8)x + (\mu_1 C_{12}+\mu_2 C_{22}+\mu_3 C_{23})y\\ &\quad + \tfrac{1}{2}\big((\mu_5/a)C_{23} - (\mu_4/b)C_{11}\big)x^2 + (\mu_5/a)C_{22}xy + \tfrac{1}{2}(\mu_4/b)C_{12}y^2. \end{aligned} \tag{13}$$

with $\omega_6 = -b^2C_{13}\mu_4/b + (b^2C_{22} - a^2C_{12})(\mu_5/a)$ and $\omega_7 = (a^2C_{11} - b^2C_{12})(\mu_4/b) - a^2C_{23}\mu_5/a$. The constant terms in u_x and u_y, which do not affect strains and stresses, have been adjusted to get relatively simple terms in columns 4 through 8 of the matrix $\mathbf{T}_+$ below. Physically, (13) aligns the bending deformation patterns along the $\{x, y\}$ axes. Evaluating (13) at the nodes we obtain the matrix that connects node displacements to stress parameters: $\mathbf{u} = \mathbf{T}_+\boldsymbol{\mu}_+$, where

$$\mathbf{T}_+ = \tfrac{1}{4}\begin{bmatrix} -2aC_{11}-bC_{13} & -2aC_{12}-bC_{23} & -2aC_{13}-bC_{33} & aC_{11} & 0 & 4a & 0 & 2b\\ -2bC_{12}-aC_{13} & -2bC_{22}-aC_{23} & -2bC_{23}-aC_{33} & 0 & bC_{22} & 0 & 4b & -2a\\ 2aC_{11}-bC_{13} & 2aC_{12}-bC_{23} & 2aC_{13}-bC_{33} & -aC_{11} & 0 & 4a & 0 & 2b\\ -2bC_{12}+aC_{13} & -2bC_{22}+aC_{23} & -2bC_{23}+aC_{33} & 0 & -bC_{22} & 0 & 4b & 2a\\ 2aC_{11}+bC_{13} & 2aC_{12}+bC_{23} & 2aC_{13}+bC_{33} & aC_{11} & 0 & 4a & 0 & -2b\\ 2bC_{12}+aC_{13} & 2bC_{22}+aC_{23} & 2bC_{23}+aC_{33} & 0 & bC_{22} & 0 & 4b & 2a\\ -2aC_{11}+bC_{13} & -2aC_{12}+bC_{23} & -2aC_{13}+bC_{33} & -aC_{11} & 0 & 4a & 0 & -2b\\ 2bC_{12}-aC_{13} & 2bC_{22}-aC_{23} & 2bC_{23}-aC_{33} & 0 & -bC_{22} & 0 & 4b & -2a\end{bmatrix} \tag{14}$$

The determinant of $\mathbf{T}_+$ is $a^4b^4C_{11}C_{22}\det(\mathbf{C})$, so $\mathbf{T}_+$ is invertible if $a \neq 0$, $b \neq 0$,

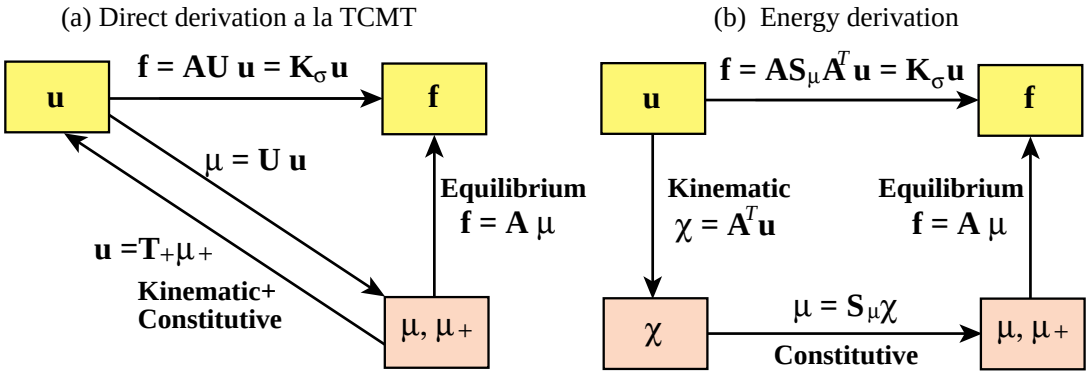

Figure 4. Derivation of the stress-assumed rectangular panel stiffness. Left side shows derivation bypassing energy methods.

$C_{11} \neq 0$, $C_{22} \neq 0$ and $\mathbf{C}$ is nonsingular. Inversion yields $\boldsymbol{\mu}_+ = \mathbf{U}_+\mathbf{u}$, where

$$\mathbf{U}_+ = \mathbf{T}_+^{-1} = \frac{1}{ab}\begin{bmatrix} U_{11} & U_{12} & U_{13} & U_{14} & U_{15} & U_{16} & U_{17} & U_{18} \\ U_{21} & U_{22} & U_{23} & U_{24} & U_{25} & U_{26} & U_{27} & U_{28} \\ U_{31} & U_{32} & U_{33} & U_{34} & U_{35} & U_{36} & U_{37} & U_{38} \\ bC_{11}^{-1} & 0 & -bC_{11}^{-1} & 0 & bC_{11}^{-1} & 0 & -bC_{11}^{-1} & 0 \\ 0 & aC_{22}^{-1} & 0 & -aC_{22}^{-1} & 0 & aC_{22}^{-1} & 0 & -aC_{22}^{-1} \\ \frac{1}{4}b & 0 & \frac{1}{4}b & 0 & \frac{1}{4}b & 0 & \frac{1}{4}b & 0 \\ 0 & \frac{1}{4}a & 0 & \frac{1}{4}a & 0 & \frac{1}{4}a & 0 & \frac{1}{4}a \\ \frac{1}{4}a & -\frac{1}{4}b & \frac{1}{4}a & \frac{1}{4}b & -\frac{1}{4}a & \frac{1}{4}b & -\frac{1}{4}a & -\frac{1}{4}b \end{bmatrix}, \tag{15}$$

in which $U_{11} = -\frac{1}{2}(bE_{11}+aE_{13})$, $U_{12} = -\frac{1}{2}(aE_{12}+bE_{13})$, $U_{13} = \frac{1}{2}(bE_{11}-aE_{13})$, $U_{14} = -\frac{1}{2}(aE_{12}-bE_{13})$, $U_{15} = \frac{1}{2}(bE_{11}+aE_{13})$, $U_{16} = \frac{1}{2}(aE_{12}+bE_{13})$, $U_{17} = -\frac{1}{2}(bE_{11}-aE_{13})$, $U_{18} = \frac{1}{2}(aE_{12}-bE_{13})$, $U_{21}=-\frac{1}{2}(bE_{12}+aE_{23})$, $U_{22}=-\frac{1}{2}(aE_{22}+bE_{23})$, $U_{23} = \frac{1}{2}(bE_{12}-aE_{23})$, $U_{24} = -\frac{1}{2}(aE_{22}-bE_{23})$, $U_{25} = \frac{1}{2}(bE_{12}+aE_{23})$, $U_{26} = \frac{1}{2}(aE_{22}+bE_{23})$, $U_{27} = -\frac{1}{2}(bE_{12}-aE_{23})$, $U_{28} = \frac{1}{2}(aE_{22}-bE_{23})$, $U_{31} = -\frac{1}{2}(bE_{13}+aE_{33})$, $U_{32} = -\frac{1}{2}(aE_{23}+bE_{33})$, $U_{33} = \frac{1}{2}(bE_{13}-aE_{33})$, $U_{34} = -\frac{1}{2}(aE_{23}-bE_{33})$, $U_{35} = \frac{1}{2}(bE_{13}+aE_{33})$, $U_{36} = \frac{1}{2}(aE_{23}+bE_{33})$, $U_{37} = -\frac{1}{2}(bE_{13}-aE_{33})$ and $U_{38} = \frac{1}{2}(aE_{23}-bE_{33})$. The stress-displacement matrix $\mathbf{U}$ that relates stress parameters to displacements: $\boldsymbol{\mu} = \mathbf{U}\,\mathbf{u}$, is obtained by extracting the first five rows of $\mathbf{U}_+$:

$$\mathbf{U} = \frac{1}{ab}\begin{bmatrix} U_{11} & U_{12} & U_{13} & U_{14} & U_{15} & U_{16} & U_{17} & U_{18} \\ U_{21} & U_{22} & U_{23} & U_{24} & U_{25} & U_{26} & U_{27} & U_{28} \\ U_{31} & U_{32} & U_{33} & U_{34} & U_{35} & U_{36} & U_{37} & U_{38} \\ bC_{11}^{-1} & 0 & -bC_{11}^{-1} & 0 & bC_{11}^{-1} & 0 & -bC_{11}^{-1} & 0 \\ 0 & aC_{22}^{-1} & 0 & -aC_{22}^{-1} & 0 & aC_{22}^{-1} & 0 & -aC_{22}^{-1} \end{bmatrix} = \mathbf{S}_\mu\,\mathbf{A}^T. \tag{16}$$

The relation $\mathbf{U} = \mathbf{S}_\mu\mathbf{A}^T$ can be checked directly. For this element it can be proven to hold by energy methods, but that was not obvious in 1952. It must have been a relief when the element stiffness came out symmetric. As Gallagher[8] remarks on p. 22, symmetry is the exception rather than the rule for more general geometric configurations. That complication proved a big boost for the energy and variational methods of the second generation.

The physical stiffness $\mathbf{K}_\sigma$ relates $\mathbf{f} = \mathbf{K}_\sigma\,\mathbf{u}$, where the σ subscript flags the stress

element. Combining $\mathbf{f} = \mathbf{A}\,\boldsymbol{\mu}$ and $\boldsymbol{\mu} = \mathbf{U}\,\mathbf{u} = \mathbf{S}_\mu\,\mathbf{A}^T\,\mathbf{u}$ yields

$$\mathbf{K}_\sigma = \mathbf{A}\,\mathbf{U} = \mathbf{A}\,\mathbf{S}_\mu\,\mathbf{A}^T. \tag{17}$$

Figure 4 summarizes the foregoing derivation steps. Note that one can bypass the calculation of the generalized stiffness $\mathbf{S}_\mu$ if so desired, as diagramed on the left of that figure. This is convenient for presentation to students without a background on energy methods.

Note that the displacement field (13) contains quadratic terms if μ_4 or μ_5 are nonzero. Hence the element is nonconforming. This is acknowledged but dismissed as innocuous on p. 814 of TCMT.

5 THE STRAIN ELEMENT

A strain-assumed element can be developed through an entirely analogous procedure. The counterpart of (6) is

$$e_{xx} = \chi_1 + \chi_4\,\frac{y}{b}, \qquad e_{yy} = \chi_2 + \chi_5\,\frac{x}{a}, \qquad 2e_{xy} = \chi_3. \tag{18}$$

where the χ_i are dimensionless strain-amplitude parameters. They are collected in the 5-vector

$$\boldsymbol{\chi} = [\ \chi_1 \quad \chi_2 \quad \chi_3 \quad \chi_4 \quad \chi_5\ ]^T\ . \tag{19}$$

An extended vector is constructed by appending the RBM amplitudes

$$\boldsymbol{\chi}_+ = [\ \chi_1 \quad \chi_2 \quad \chi_3 \quad \chi_4 \quad \chi_5 \quad \chi_6 \quad \chi_7 \quad \chi_8\ ]^T\ . \tag{20}$$

in which χ_6, χ_7 and χ_8 are defined a a manner similar to (9). Note that $\mathbf{e} = \mathbf{N}\boldsymbol{\chi} = \mathbf{N}_+\boldsymbol{\chi}_+$ where $\mathbf{N}$ and $\mathbf{N}_+$ are defined in (10). Integrating the strains yields the displacement field

$$\begin{aligned} u_x(x,y) &= \chi_6 + \chi_8 y + (\chi_1 + \chi_4/b)xy - \tfrac{1}{2}(\chi_5/a)y^2,\\ u_y(x,y) &= \chi_7 + (\chi_3 - \chi_8)x + \chi_2 y - \tfrac{1}{2}(\chi_4/b)x^2 + (\chi_5/a)xy. \end{aligned} \tag{21}$$

Evaluating at the nodes and inverting yields $\boldsymbol{\chi}_+ = \mathbf{B}_+\mathbf{u}$ where

$$\mathbf{B}_+ = \frac{1}{8ab}\begin{bmatrix} -4b & 0 & 4b & 0 & 4b & 0 & -4b & 0\\ 0 & -4a & 0 & -4a & 0 & 4a & 0 & 4a\\ -4a & -4b & -4a & 4b & 4a & 4b & 4a & -4b\\ 8b & 0 & -8b & 0 & 8b & 0 & -8b & 0\\ 0 & 8a & 0 & -8a & 0 & 8a & 0 & -8a\\ 2ab & b^2 & 2ab & -b^2 & 2ab & b^2 & 2ab & -b^2\\ a^2 & 2ab & -a^2 & 2ab & a^2 & 2ab & -a^2 & 2ab\\ -4a & 0 & -4a & 0 & 4a & 0 & 4a & 0 \end{bmatrix} \tag{22}$$

from which we extract the first five rows to get the strain-displacement matrix relating $\boldsymbol{\chi} = \mathbf{B}_\chi\mathbf{u}$:

$$\mathbf{B}_\chi = \frac{h}{2V}\begin{bmatrix} -b & 0 & b & 0 & b & 0 & -b & 0\\ 0 & -a & 0 & -a & 0 & a & 0 & a\\ -a & -b & -a & b & a & b & a & -b\\ 2b & 0 & -2b & 0 & 2b & 0 & -2b & 0\\ 0 & 2a & 0 & -2a & 0 & 2a & 0 & -2a \end{bmatrix} \tag{23}$$

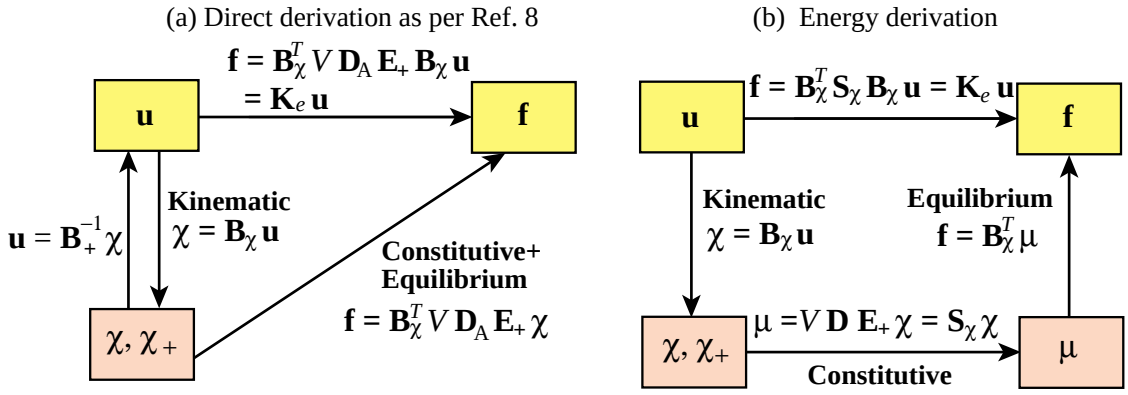

Figure 5. Derivation of the strain-assumed rectangular panel stiffness. Left diagram shows derivation bypassing energy methods.

For use below we note the following relation between the transformation matrices of the stress and strain elements

$$\mathbf{A}^T = V\,\mathbf{D}_A\,\mathbf{B}_\chi,\quad \mathbf{B}_\chi = \frac{1}{V}\mathbf{D}_A^{-1}\mathbf{A}^T,\quad \mathbf{D}_A = \begin{bmatrix} 1 & 0 & 0 & 0 & 0\\ 0 & 1 & 0 & 0 & 0\\ 0 & 0 & 1 & 0 & 0\\ 0 & 0 & 0 & \frac{1}{12} & 0\\ 0 & 0 & 0 & 0 & \frac{1}{12}\end{bmatrix} = \begin{bmatrix} \mathbf{I}_3 & \mathbf{0}\\ \mathbf{0} & \frac{1}{12}\mathbf{I}_2\end{bmatrix} = \mathbf{D}_A^T. \tag{24}$$

From (11) the lumping of the slave stress field $\mathbf{Ee} = \mathbf{EN}\boldsymbol{\chi}$ to node forces can be worked out to be

$$\mathbf{f} = \mathbf{A}\mathbf{E}_+\boldsymbol{\chi} = V\,\mathbf{B}_\chi^T\mathbf{D}_A\mathbf{E}_+\boldsymbol{\chi},\quad \text{with}\quad \mathbf{E}_+ = \begin{bmatrix} E_{11} & E_{12} & E_{13} & 0 & 0\\ E_{12} & E_{22} & E_{23} & 0 & 0\\ E_{13} & E_{23} & E_{33} & 0 & 0\\ 0 & 0 & 0 & E_{11} & 0\\ 0 & 0 & 0 & 0 & E_{22}\end{bmatrix} \tag{25}$$

Combining previous equations, the physical element stiffness is

$$\mathbf{K}_e = V\,\mathbf{B}_\chi^T\mathbf{D}_A\mathbf{E}_+\mathbf{B}_\chi = \mathbf{B}_\chi^T\mathbf{K}_\chi\mathbf{B}_\chi,\quad \text{with}\quad \mathbf{K}_\chi = V\,\mathbf{D}_A\mathbf{E}_+. \tag{26}$$

Here $\mathbf{K}_\chi$ denotes the generalized stiffness in terms of $\boldsymbol{\chi}$. This matrix may be obtained also from standard energy arguments: the strain energy density is $\mathcal{U} = \frac{1}{2}\boldsymbol{\chi}^T\mathbf{E}\boldsymbol{\chi}$. Integrating over the element volume: $U = \int_{V^e}\mathcal{U}\,dV$ and identifying with $\frac{1}{2}\boldsymbol{\chi}^T\mathbf{K}_\chi\boldsymbol{\chi}$ gives

$$\mathbf{K}_\chi = V\,\mathbf{D}_A\mathbf{E}_+ = V\begin{bmatrix} E_{11} & E_{12} & E_{13} & 0 & 0\\ E_{12} & E_{22} & E_{23} & 0 & 0\\ E_{13} & E_{23} & E_{33} & 0 & 0\\ 0 & 0 & 0 & \frac{1}{12}E_{11} & 0\\ 0 & 0 & 0 & 0 & \frac{1}{12}E_{22}\end{bmatrix} \tag{27}$$

Figure 5 summarizes the foregoing derivation steps. The direct step from $\boldsymbol{\chi}$ to $\mathbf{f}$ on the left is more difficult to explain to students than the step from $\mathbf{u}$ to $\boldsymbol{\mu}$ in Figure 4. The energy based formulation shown on the right of Figure 5 tends to be more palatable.

6 THE CONFORMING DISPLACEMENT ELEMENT

This derivation of the assumed-displacement element starts from a conforming displacement field that enforces linear edge displacements. Using the matrix notation of Felippa and Clough[66] for Irons' isoparametric formulation[25] specialized to the rectangle, the displacement field is bilinearly interpolated as

$$\begin{bmatrix} u_x(x,y) \\ u_y(x,y) \end{bmatrix} = \tfrac{1}{2}\begin{bmatrix} -a & 0 & a & 0 & a & 0 & -a & 0 \\ 0 & -b & 0 & -b & 0 & b & 0 & b \end{bmatrix} \begin{bmatrix} \frac{1}{4}(1-\xi)(1-\eta) \\ \frac{1}{4}(1+\xi)(1-\eta) \\ \frac{1}{4}(1+\xi)(1+\eta) \\ \frac{1}{4}(1-\xi)(1+\eta) \end{bmatrix}, \tag{28}$$

where $\xi = 2x/a$ and $\eta = 2y/b$ are the dimensionless quadrilateral coordinates running from -1 to 1. The derivation based on the minimum potential energy principle is standard textbook material and only the final result is presented here:

$$\mathbf{K}_u = \mathbf{B}_u^T \mathbf{K}_q \mathbf{B}_u, \quad \text{with} \quad \mathbf{K}_q = \frac{1}{V}\begin{bmatrix} E_{11} & E_{12} & E_{13} & 0 & 0 \\ E_{12} & E_{22} & E_{23} & 0 & 0 \\ E_{13} & E_{23} & E_{33} & 0 & 0 \\ 0 & 0 & 0 & Q_{11} & Q_{12} \\ 0 & 0 & 0 & Q_{12} & Q_{22} \end{bmatrix}, \tag{29}$$

in which $\mathbf{B}_u = \mathbf{A}^T$ as given by (11) and

$$Q_{11} = 12\frac{b^2E_{11} + a^2E_{33}}{ab^3h}, \quad Q_{12} = 12\left(\frac{E_{13}}{a^2h} + \frac{E_{23}}{b^2h}\right), \quad Q_{22} = 12\frac{a^2E_{22} + b^2E_{33}}{a^3bh} \tag{30}$$

This model has a checkered history. It was first derived as a rectangular panel with edge reinforcements (omitted here) by Argyris in his 1954 *Aircraft Engineering* series; see pp. 49–52 of the Butterworths reprint.[5] Argyris used bilinear displacement interpolation in Cartesian coordinates. After much flailing, a conforming generalization to arbitrary geometry was published in 1964 by Taig and Kerr[67] using quadrilateral-fitted coordinates called $\{\xi, \eta\}$ but running from 0 to 1. This paper cites an 1961 English Electric Aircraft internal report as original source but Irons and Ahmad[25] comment in their reference [108] that the work goes back to 1957.) Irons, who was aware of Taig's work while at Rolls Royce, created the seminal isoparametric family as a far-reaching extension upon moving to Swansea.[21–24]

7 TEMPLATES

7.1 Stiffness Decomposition

The stiffnesses $\mathbf{K}_\sigma$, $\mathbf{K}_e$ and $\mathbf{K}_u$ derived in the foregoing three Sections do not appear to have much in common. Indeed if one looks at just the matrix entries no pattern is readily seen. Closer examination reveals, however, that they are instances of the algebraic form

$$\mathbf{K} = \mathbf{K}_b + \mathbf{K}_h = V\,\mathbf{H}_c^T\mathbf{E}\mathbf{H}_c + V\,\mathbf{H}_h^T\mathbf{W}^T\mathbf{R}\mathbf{W}\mathbf{H}_h, \tag{31}$$

where $V = abh$ is the element volume and

$$\begin{aligned} \mathbf{H}_c &= \frac{1}{2ab}\begin{bmatrix} -b & 0 & b & 0 & b & 0 & -b & 0 \\ 0 & -a & 0 & -a & 0 & a & 0 & a \\ -a & -b & -a & b & a & b & a & -b \end{bmatrix}, \\ \mathbf{H}_h &= \tfrac{1}{2}\begin{bmatrix} 1 & 0 & -1 & 0 & 1 & 0 & -1 & 0 \\ 0 & 1 & 0 & -1 & 0 & 1 & 0 & -1 \end{bmatrix}, \\ \mathbf{W} &= \begin{bmatrix} 1/a & 0 \\ 0 & 1/b \end{bmatrix}, \quad \mathbf{R} = \begin{bmatrix} R_{11} & R_{12} \\ R_{12} & R_{22} \end{bmatrix}. \end{aligned} \tag{32}$$

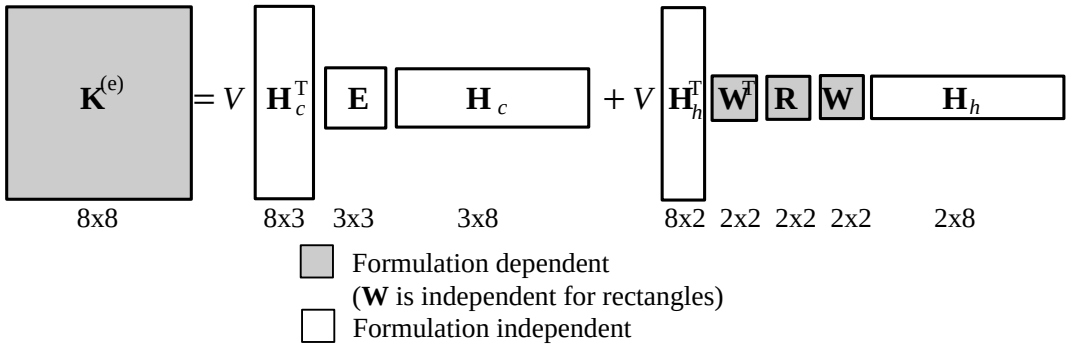

Figure 6. The template for the rectangular panel, illustrating formulation dependent and independent parts.

Matrices $\mathbf{H}_c$ and $\mathbf{H}_h$ are identical for the three models. The generalized bending rigidity $\mathbf{R}$ is formulation dependent. Matrix $\mathbf{W}$ is a "higher-order-mode weighting matrix," hence the notation. For rectangular panels $\mathbf{W}$ is diagonal and formulation independent. For more complex geometries discussed in the Appendix and in the sequel[3] $\mathbf{W}$ may be formulation-adjusted to make $\mathbf{R}$ simpler.

For the stress, strain and displacement models $\mathbf{R}$ becomes $\mathbf{R}_\sigma$, $\mathbf{R}_e$ and $\mathbf{R}_u$, respectively, where

$$\mathbf{R}_\sigma = \tfrac{1}{3}\begin{bmatrix} C_{11}^{-1} & 0 \\ 0 & C_{22}^{-1} \end{bmatrix},\ \mathbf{R}_e = \tfrac{1}{3}\begin{bmatrix} E_{11} & 0 \\ 0 & E_{22} \end{bmatrix},\ \mathbf{R}_u = \tfrac{1}{3}\begin{bmatrix} E_{11} + \dfrac{a^2 E_{33}}{b^2} & \dfrac{bE_{13}}{a} + \dfrac{aE_{23}}{b} \\ \dfrac{bE_{13}}{a} + \dfrac{aE_{23}}{b} & E_{22} + \dfrac{b^2 E_{33}}{a^2} \end{bmatrix} \tag{33}$$

But we are not in fact restricted to these. Other expressions for $\mathbf{R}$ would yield other $\mathbf{K}$. These are possible, although not necessarily useful, stiffnesses for the rectangular panel if $\mathbf{R}$ is symmetric and positive definite, and if its entries have physical dimensions of elastic moduli. Further if $E_{13} = E_{23} = 0$ we set $R_{12} = 0$. The key discovery is that the element formulation affects only part of the stiffness expression, as highlighted in Figure 6.

7.2 Template Terminology

The algebraic form characterized by (31) and (32) is called a finite element stiffness template, or *template* for short.

Matrices $\mathbf{K}_b$ and $\mathbf{K}_h$ are called the basic and higher-order stiffness matrix, respectively, in accordance with the fundamental decomposition of the Free Formulation.[41,42,58–65] These two matrices play different and complementary roles.

The basic stiffness $\mathbf{K}_b$ takes care of consistency and mixability. In the Free Formulation a restatement of (31) is preferred:

$$\mathbf{K}_b = V^{-1}\,\mathbf{L}\,\mathbf{E}\,\mathbf{L}^T, \tag{34}$$

where $\mathbf{L} = \mathbf{H}_c / V$ is called the force lumping matrix, or simply lumping matrix.

The higher order stiffness $\mathbf{K}_h$ is a *stabilization* term that provides the correct rank and may be adjusted for accuracy. This matrix is orthogonal to rigid body motions and constant strain states. To verify the claim for this particular template introduce the following 8×6

```
RectPanel4TemplateStiffness[{a_,b_},Emat_,Cmat_,h_,name_,Rlist_]:=
  Module[{V,found,Hc,Hh,W,Ke}, V=a*b*h;
  {WRW,found}=RectPanel4TemplateWRW[{a,b},Emat,Cmat,name,Rlist];
  If [Not[found], Print["Illegal elem name: ",name]; Abort[]];
  Hc={{-b,0,b,0,b,0,-b,0}, {0,-a,0,-a,0,a,0,a},
      {-a,-b,-a,b,a,b,a,-b}}/(2*a*b);
  Hh={{1,0,-1,0,1,0,-1,0},{0,1,0,-1,0,1,0,-1}}/2;
  Ke=V*Transpose[Hc].Emat.Hc+V*Transpose[Hh].WRW.Hh;
  Return[Simplify[Ke]]];

RectPanel4TemplateWRW[{a_,b_},Emat_,Cmat_,name_,Rlist_]:=
 Module[{R11,R12,R22,Rmat,E11,E12,E13,E22,E23,E33,
 found=False,C11,C22,C33,C12,C13,C23,Edet,Cdet,W,WRW},
  {{E11,E12,E13},{E12,E22,E23},{E13,E23,E33}}=Emat;
  If [Length[Cmat]<=0,
     Edet=E11*E22*E33+2*E12*E13*E23-E11*E23^2-E22*E13^2-E33*E12^2;
     C11=(E22*E33-E23^2)/Edet; C22=(E11*E33-E13^2)/Edet;
     C33=(E11*E22-E12^2)/Edet; C12=(E13*E23-E12*E33)/Edet;
     C13=(E12*E23-E13*E22)/Edet; C23=(E12*E13-E11*E23)/Edet,
     {{C11,C12,C13},{C12,C22,C23},{C13,C23,C33}}=Cmat,
     {{C11,C12,C13},{C12,C22,C23},{C13,C23,C33}}=Cmat];
  If [name=="Stress"||name=="QM6"||name=="Q6",
     R11=1/(3*C11); R22=1/(3*C22); R12=0; found=True];
  If [name=="Strain", R11=E11/3; R22=E22/3; R12=0; found=True];
  If [name=="Disp",  R11=(E11+E33*a^2/b^2)/3;
     R22=(E22+E33*b^2/a^2)/3; R12=(E13*b/a+E23*a/b)/3; found=True];
  If [name=="Arbitrary", {R11,R12,R22}=Rlist; found=True];
  W={{1/a,0},{0,1/b}}; Rmat={{R11,R12},{R12,R22}};
  WRW=Transpose[W].Rmat.W; Return[{WRW,found}]];
```

Figure 7. A *Mathematica* implementation of the rectangular panel template (31).

matrix, called the basic-mode matrix in the Free Formulation:

$$\mathbf{G}_{rc} = \begin{bmatrix} 1 & 0 & y_1 & x_1 & 0 & y_1 \\ 0 & 1 & -x_1 & 0 & y_1 & x_1 \\ 1 & 0 & y_2 & x_2 & 0 & y_2 \\ 0 & 1 & -x_2 & 0 & y_2 & x_2 \\ 1 & 0 & y_3 & x_3 & 0 & y_3 \\ 0 & 1 & -x_3 & 0 & y_3 & x_3 \\ 1 & 0 & y_4 & x_4 & 0 & y_4 \\ 0 & 1 & -x_4 & 0 & y_4 & x_4 \end{bmatrix} = \tfrac{1}{2} \begin{bmatrix} 2 & 0 & -b & -a & 0 & -b \\ 0 & 2 & a & 0 & -b & -a \\ 2 & 0 & -b & a & 0 & -b \\ 0 & 2 & -a & 0 & -b & a \\ 2 & 0 & b & a & 0 & b \\ 0 & 2 & -a & 0 & b & a \\ 2 & 0 & b & -a & 0 & b \\ 0 & 2 & a & 0 & b & -a \end{bmatrix}. \tag{35}$$

The six columns of $\mathbf{G}_{rc}$ span the rigid body modes and constant strain states evaluated at the nodes (these bases are not orthonormalized as that property is not required here). It is readily checked that $\mathbf{H}_h\mathbf{G}_{rc} = \mathbf{0}$. Therefore those modes, and any linear combination thereof, are orthogonal to the higher order stiffness: $\mathbf{K}_h\mathbf{G}_{rc} = \mathbf{0}$. So the role of $\mathbf{H}_h$ is essentially that of a *geometric projector*.

A *Mathematica* implementation of (31) as module `RectPanel4TemplateStiffness` is shown in Figure 7. The module arguments are the rectangle dimensions as list `{a,b}`, the elasticity matrix as list `Emat={{E11,E12,E13},{E12,E22,E23},{E13,E23,E33}}`, the compliance matrix as `Cmat={{C11,C12,C13},{C12,C22,C23},{C13,C23,C33}}`, the thickness `h`, the name as one of `"Stress"` ,`"Strain"`, `"Disp"`, `"Q6"`, `"QM6"` or `"Arbitrary"`, and finally the list `Rlist={R11,R12,R22}`. The latter is used if the name is `"Arbitrary"`. This comes handy for finding the signature of known elements leaving the entries of `Rlist` symbolic and using the `Solve` command to match existing or new

Table 1. A Clone Gallery

Name	Description	Clones and sources
StressRP (a.k.a. BORP)	5-stress-mode element of Section 4	Direct derivation: TCMT[1], Gallagher[8] Pian 5-mode stress hybrid[27,26,29] Wilson-Taylor-Doherty-Ghaboussi Q6[68] Taylor-Wilson-Beresford QM6[69] Belytschko-Liu-Engelmann QBI[70] SRI of iso-P with **E** split as per (54)
StrainRP	5-strain-mode element of Section 5	MacNeal QUAD4[39,71] SRI of iso-P with **E** split as per (56)
DispRP	Bilinear iso-P element of Section 6	Argyris[5] as edge stiffened rectangular panel Taig-Kerr[67] as specialized quadrilateral

Note 1: Many plane stress models listed above were derived for quadrilateral geometries, and a few as membrane component of shells. The right-hand-column classification only pertains to the rectangular panel specialization. For example, Q6 and QM6 differ for non-parallelogram shapes.
Note 2: Instances of the stress-hybrid and displacement-bubble-function "futile families" studied in Section 11 are omitted, as they lack practical value.
Note 3: Post-1990 clones (e.g. EAS[54]) omitted to save space. See Lautersztajn and Samuelsson[72] for a recent survey.

elements. If `Cmat` is supplied as the empty list { }, the compliance matrix is calculated internally as inverse of `Emat`.

The module returns the 8×8 stiffness matrix `Ke` as function value. To get the basic stiffness $\mathbf{K}_b$ only, call with `name = "Arbitrary"` and `Rlist={0,0,0}`.

7.3 Requirements

An acceptable template fulfills four conditions: (C) consistency, (S) stability (correct rank), (I) observer invariance and (P) parametrization. These are discussed at length in other papers.[73–79] Conditions (C) and (S) are imposed to ensure convergence as the mesh size is reduced by enforcing *a priori* satisfaction of the Individual Element Test (IET) of Bergan and Hanssen.[56,57] Condition (P) means that the template contains free parameters or free matrix entries. In the case of (31), the simplest choice of parameters are the entries R_{11}, R_{12}, R_{22} themselves. To fulfill stability, $R_{11} > 0$, $R_{22} > 0$ and $R_{11}R_{22} - R_{12}^2 > 0$. Parametrization facilitates performance optimization as well as tuning elements, or combinations of elements, to fulfill specific needs.

Using the IET as departure point it is not difficult to show[80] that (31), under the stated restrictions on **R**, includes all stiffnesses that satisfy the IET and stability. Observer invariance is a moot point for this element since $\{x, y\}$ are side aligned. Thus (31) is in fact a universal template for the rectangular panel.

7.4 Instances, Signatures, Clones

Setting the free parameters to specific values yields element instances. The set of free parameters is called the template *signature*, a term introduced in previous papers.[77,78] Borrowing terminology from biogenetics, the signature may be viewed as an "element DNA" that uniquely characterizes it as an individual entity. Elements derived by different techniques that share the same signature are called *clones*.

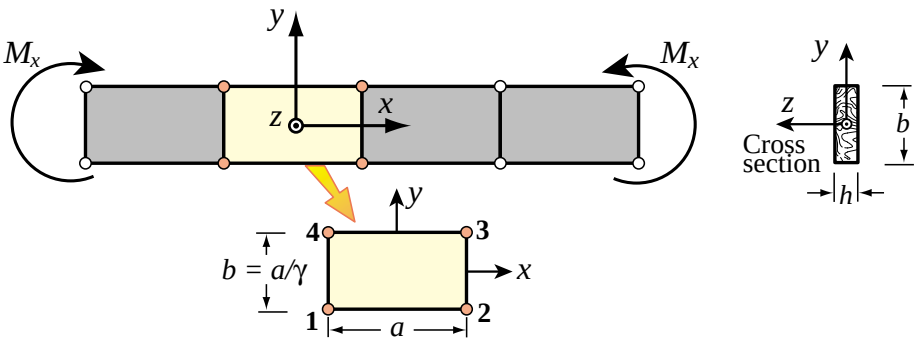

Figure 8. Constant-moment inplane-bending test along the x side dimension.

One of the "template services" is automatic identification of clones. If two elements fitting the template (31) share R_{11}, R_{12} and R_{22}, they are clones. Inasmuch as most FEM formulation schemes have been tried on the rectangular panel, it should come as no surprise that there are many clones, particularly of the stress element. Those published before 1990 are collected in Table 1. For example, the incompatible mode element Q6 of Wilson et al.[68] is a clone of StressRP. The version QM6 of Taylor et al.[69] which passes the patch test for arbitrary geometries, reduces to Q6 for rectangular and parallelogram shapes. Even for this simple geometry recognition of some of the coalescences took some time, as recently narrated by Pian.[29]

8 FINDING THE BEST

An universal template is nice to have. The obvious question arises: among the infinity of elements that it can generate, is there a best one? By construction all instances verify exactly the IET for rigid body modes and uniform strain states. Hence the optimality criterion must rely on higher order patch tests.

8.1 The Bending Tests

The obvious tests involve response to in-plane bending along the side directions. This leads to comparisons in the form of energy ratios. These have been used since 1984 to tune up the higher order stiffness of triangular elements.[58–62,81] An extension introduced in this article is consideration of arbitrary anisotropic material. All symbolic calculations were carried out with *Mathematica*.

The x bending test is depicted in Figure 8. A Bernoulli-Euler plane beam of thin rectangular cross-section with height b and thickness h (normal to the plane of the figure) is bent under applied end moments M_x. The beam is fabricated of anisotropic material with the stress-strain law $\boldsymbol{\sigma} = \mathbf{E}\boldsymbol{\varepsilon}$ of $(2)_2$. Except for possible end effects the exact solution of the beam problem (from both the theory-of-elasticity and beam-theory standpoints) is a constant bending moment $M(x) = M_x$ along the span. The associated stress field is $\sigma_{xx} = -M_x\, y/I_b$, $\sigma_{yy} = \sigma_{xy} = 0$, where $I_b = \frac{1}{12}hb^3$.

For the y bending test, depicted in Figure 9, the beam cross section has height a and thickness h, and is subjected to end moments M_y. The exact solution is $M(y) = M_y$. The associated stress field is $\sigma_{yy} = M_y\, x/I_a$ and $\sigma_{xx} = \sigma_{xy} = 0$, where $I_a = \frac{1}{12}ha^3$. For comparing with the FEM discretizations below, the internal (complementary) energies taken up by beam segments of lengths a and b in the configurations of Figures 8 and 9, respectively, are

$$U_x^{\text{beam}} = \frac{6aC_{11}M_x^2}{b^3h}, \qquad U_y^{\text{beam}} = \frac{6bC_{22}M_y^2}{a^3h} \tag{36}$$

For the 2D element tests, each beam is modeled with one layer of identical 4-node rectangular panels dimensioned $a \times b$ as shown in Figures 8 and 9. The aspect ratio b/a is denoted by γ. By analogy with the exact solution, all rectangles in the finite element model will undergo the same deformations and stresses. We can therefore consider a typical element. For x bending the exact stress distribution is represented by (7) on taking $\mu_4 = -M_x b/I_b = -12M_x/(b^2 h)$ and $\mu_1 = \mu_2 = \mu_3 = \mu_5 = 0$. The rigid body mode amplitudes are chosen to be zero for convenience: $\mu_6 = \mu_7 = \mu_8 = 0$. Inserting these μ_i into (14) we get the node displacement vector

$$\mathbf{u}_{bx} = \frac{12M_x C_{11} a}{b^2 h}\,[\,-1 \quad 0 \quad 1 \quad 0 \quad -1 \quad 0 \quad 1 \quad 0\,]^T\,. \tag{37}$$

Likewise, for the y bending test the element stress field is obtained by taking $\mu_5 = M_y a/I_a = 12M_y/(a^2 h)$ and $\mu_1 = \mu_2 = \mu_3 = \mu_4 = \mu_6 = \mu_7 = \mu_8 = 0$. The node displacement vector given by (14) is

$$\mathbf{u}_{by} = \frac{12M_y C_{22} b}{a^2 h}\,[\,0 \quad 1 \quad 0 \quad -1 \quad 0 \quad 1 \quad 0 \quad -1\,]^T\,. \tag{38}$$

The strain energies absorbed by the panel element under these applied node displacements are $U_x^{\text{panel}} = \frac{1}{2}\mathbf{u}_{bx}^T \mathbf{K} \mathbf{u}_{bx}$ and $U_y^{\text{panel}} = \frac{1}{2}\mathbf{u}_{by}^T \mathbf{K} \mathbf{u}_{by}$, respectively. Define the bending energy ratios as

$$r_x = \frac{U_x^{\text{panel}}}{U_x^{\text{beam}}}, \quad r_y = \frac{U_y^{\text{panel}}}{U_y^{\text{beam}}}. \tag{39}$$

These happen to be the ratios of the exact (beam) displacement solution to that of the rectangular panel solution. Hence $r_x = 1$ means that we get the exact answer under M_x, that is, the panel is x-bending exact. If $r_x > 1$ or $r_x < 1$ the panel is overstiff or overflexible in x bending, respectively. Likewise for y bending. If $r_x = 1$ and $r_y = 1$ for any aspect ratio $\gamma = b/a$ and arbitrary material properties the element is called *bending optimal*. If $r_x >> 1$ if $a >> b$ and/or $r_y >> 1$ if $a << b$ the element is said to experience *aspect ratio locking* along the x or y direction, respectively. This is called *shear locking* in the FEM literature because it is traceable to spurious shear energy, as shown in Section 8.4.

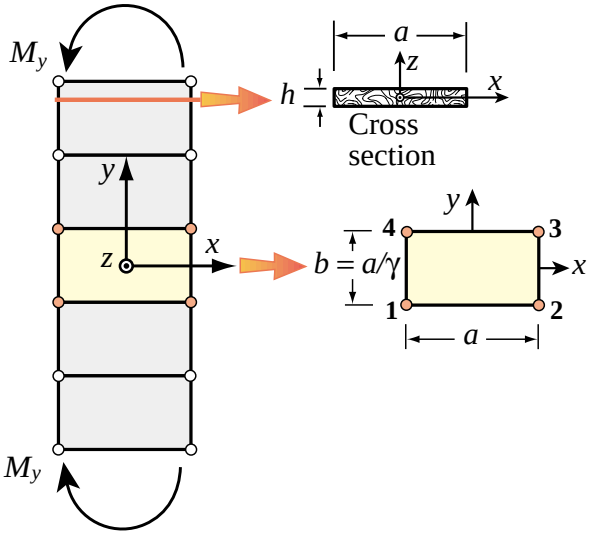

Figure 9. Constant-moment inplane-bending test along the y side dimension.

8.2 The Optimal Panel

Applying the tests to the template (31) yields

$$r_x = 3C_{11}R_{11}, \qquad r_y = 3C_{22}R_{22}. \tag{40}$$

Clearly to get $r_x = r_y = 1$ for any aspect ratio we must take

$$R_{11} = \tfrac{1}{3}C_{11}^{-1}, \quad R_{22} = \tfrac{1}{3}C_{22}^{-1} \tag{41}$$

Since R_{12} is absent from (41) one can set $R_{12} = 0$ for convenience. Comparing to the $\mathbf{R}_\sigma$ of (33) shows that the 5-parameter stress model of TCMT and its clones *is the bending-optimal rectangular panel*. For isotropic material $R_{11} = R_{22} = \frac{1}{3}E$. The StressRP template instance will be henceforth also identified by the acronym BORP, for Bending Optimal Rectangular Panel.

8.3 The Strain Element Does Not Lock

It is interesting to apply the result (40) to other template instances. The StrainRP element generated by the $\mathbf{R}_e$ of (33) gives

$$r_x = C_{11}E_{11}, \qquad r_y = C_{22}E_{22}. \tag{42}$$

If the material is isotropic, $C_{11} = C_{22} = 1/E$ and $E_{11} = E_{22} = E/(1-\nu^2)$. This yields $r_x = r_y = 1/(1-\nu^2)$, which varies between 1 and 4/3. For an orthotropic body with principal material axes aligned with the rectangle sides, $E_{11} = E_1/(1-\nu_{12}\nu_{21})$, $E_{22} = E_2/(1-\nu_{12}\nu_{21})$, $C_{11} = 1/E_1$, $C_{22} = 1/E_2$, and $r_x = r_y = 1/(1-\nu_{12}\nu_{21})$. These are independent of the aspect ratio γ. Consequently StrainRP and its clones *do not lock*, although the element is not generally optimal. Note that if $C_{11}E_{11}$ and/or $C_{22}E_{22}$ differ widely from 1, as may happen in highly anisotropic materials, the bending performance will be poor. The example of Section 12.2 displays this vividly.

8.4 But the Displacement Element Does

Instance DispRP is generated by the $\mathbf{R}_u$ of (33). Inserting its entries into (40) we get

$$\begin{aligned} r_x &= C_{11}(E_{11} + E_{33}\gamma^2) = \frac{(E_{22}E_{33} - E_{23}^2)(E_{11} + E_{33}\gamma^2)}{\det(\mathbf{E})}, \\ r_y &= C_{22}(E_{22} + E_{33}\gamma^{-2}) = \frac{(E_{11}E_{33} - E_{13}^2)(E_{22} + E_{33}\gamma^{-2})}{\det(\mathbf{E})}. \end{aligned} \tag{43}$$

in which $\det(\mathbf{E}) = E_{11}E_{22}E_{33} + 2E_{12}E_{13}E_{23} - E_{11}E_{23}^2 - E_{22}E_{13}^2 - E_{33}E_{12}^2$. For an isotropic material

$$r_x = \frac{2 + \gamma^2(1-\nu)}{2(1-\nu^2)}, \qquad r_y = \frac{1 + 2\gamma^2 - \nu}{2\gamma^2(1-\nu^2)}. \tag{44}$$

These relations clearly indicate aspect ratio locking for bending along the longest side dimension. For instance if $\nu = 0$ and $a = 10b$, whence $\gamma = a/b = 10$, then $r_x = 51$ and DispRP is over 50 times stiffer in x bending than the Bernoulli-Euler beam element. The expression (43) makes clear that *locking happens for any material law* as long as $E_{33} \neq 0$. Since this is the shear modulus, the name *shear locking* used in the FEM literature is justified.

8.5 Multiple Element Layers

Results of the energy bending test can be readily extended to predict the behavior of $2n$ ($n = 1, 2, \ldots$) identical layers of elements symmetrically placed through the beam height. If $2n$ layers are placed along the y direction in the configuration of Figure 8 and γ stays the same, the energy ratio becomes

$$r_x^{(2n)} = \frac{2^{2n} - 1 + r_x}{2^{2n}}, \tag{45}$$

where r_x is the ratio (40) for one layer. If $r_x \equiv 1$, $r_x^{2n} \equiv 1$ so bending exactness is maintained, as can be expected. For example, if $n = 1$ (two element layers), $r_x^{(2)} = (3 + r_x)/4$. The same result holds for r_y if $2n$ layers are placed along the x direction in the configuration of Figure 9.

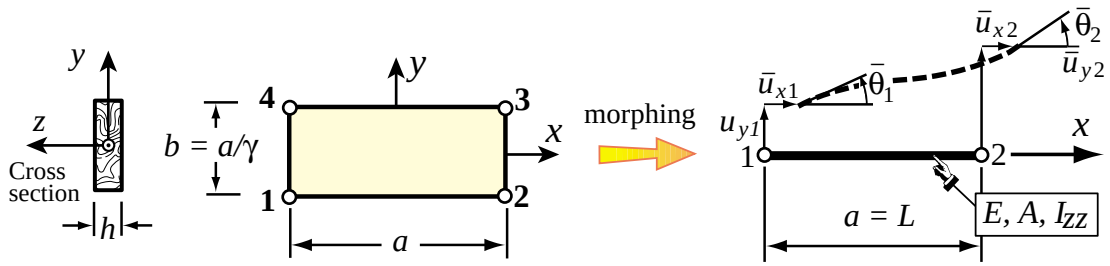

Figure 10. Morphing a 8-DOF rectangular panel unit to a 6-DOF beam-column element in the x direction.

9 MORPHING TO BEAM-COLUMN

Morphing means transforming an individual element or macroelement into a simpler model using kinematic constraints. Often the simpler element has lower dimensionality. For example a plate bending macroelement may be morphed to a Bernoulli-Euler beam or to a torqued shaft.[79] To illustrate the idea consider morphing the rectangular panel of Figure 10 into the two-node beam-column element shown on the right of that Figure. The length, cross sectional area and moment of inertia of the beam-column element, respectively, are denoted by $L = a$, $A = bh$ and $I_{zz} = b^3h/12 = a^3h/(12\gamma^3)$, respectively.

The transformation between the freedoms of the panel and those of the beam-column is

$$\mathbf{u}_R = \begin{bmatrix} u_{x1} \\ u_{y1} \\ u_{x2} \\ u_{y2} \\ u_{x3} \\ u_{y3} \\ u_{x4} \\ u_{y4} \end{bmatrix} = \begin{bmatrix} 1 & 0 & \frac{1}{2}b & 0 & 0 & 0 \\ 0 & 1 & 0 & 0 & 0 & 0 \\ 0 & 0 & 0 & 1 & 0 & \frac{1}{2}b \\ 0 & 0 & 0 & 0 & 1 & 0 \\ 0 & 0 & 0 & 1 & 0 & -\frac{1}{2}b \\ 0 & 0 & 0 & 0 & 1 & 0 \\ 1 & 0 & -\frac{1}{2}b & 0 & 0 & 0 \\ 0 & 1 & 0 & 0 & 0 & 0 \end{bmatrix} \begin{bmatrix} \bar{u}_{x1} \\ \bar{u}_{y1} \\ \bar{\theta}_1 \\ \bar{u}_{x2} \\ \bar{u}_{y2} \\ \bar{\theta}_2 \end{bmatrix} = \mathbf{T}_m \bar{\mathbf{u}}_m. \tag{46}$$

where a superposed bar distinguishes the beam-column freedoms grouped in array $\bar{\mathbf{u}}_m$. As source select StressRP fabricated of isotropic material. The morphed beam-column element stiffness is

$$\mathbf{K}_m = \mathbf{T}_m^T \mathbf{K}_\sigma \mathbf{T}_m = \frac{E}{L} \begin{bmatrix} A & 0 & 0 & -A & 0 & 0 \\ 0 & 12c_{22}I_{zz}/L^2 & 6c_{23}I_{zz}/L & 0 & -12c_{22}I_{zz}/L^2 & 6c_{23}I_{zz}/L \\ 0 & 6c_{23}I_{zz}/L & 4c_{33}I_{zz} & 0 & -6c_{23}I_{zz}/L & 4c_{33}I_{zz} \\ -A & 0 & 0 & A & 0 & 0 \\ 0 & 12c_{22}I_{zz}/L^2 & 6c_{23}I_{zz}/L & 0 & -12c_{22}I_{zz}/L^2 & 6c_{23}I_{zz}/L \\ 0 & 6c_{23}I_{zz}/L & 4c_{33}I_{zz} & 0 & -6c_{23}I_{zz}/L & 4c_{33}I_{zz} \end{bmatrix} \tag{47}$$

in which $c_{22} = c_{23} = \frac{1}{2}\gamma^2/(1+\nu)$, and $c_{33} = \frac{1}{4}(1+3c_{22})$. The entries in rows/columns 1 and 4 form the well known two-node bar stiffness. Those in rows and columns 2, 3, 5 and 6 are dimensionally homogeneous to those of a plane beam, and may be grouped into the following matrix configuration:

$$\mathbf{K}_m^{beam} = \frac{E\,I_{zz}}{L} \left(\begin{bmatrix} 0 & 0 & 0 & 0 \\ 0 & 1 & 0 & -1 \\ 0 & 0 & 0 & 0 \\ 0 & -1 & 0 & 1 \end{bmatrix} + \beta_m \begin{bmatrix} 12/L^2 & 6/L & -12/L^2 & 6/L \\ 6/L & 3 & -6/L & 3 \\ -12/L^2 & -6/L & 12/L^2 & -6/L \\ 6/L & 3 & -6/L & 3 \end{bmatrix} \right) \tag{48}$$

where $\beta_m = c_{22} = c_{23} = \frac{1}{2}\gamma^2/(1+\nu)$. But (48), with β_m replaced by a free parameter β, happens to be the universal template of a prismatic plane beam.[73] Mass-stiffness template combinations have been studied for dynamics and vibration using Fourier methods.[82,83]

The basic stiffness on the left characterizes the pure-bending symmetric response to a uniform moment, whereas the higher-order stiffness on the right characterizes the antisymmetric response to a linearly-varying, bending moment of zero mean. For the Bernoulli-Euler beam constructed with cubic shape functions, $\beta = 1$. For the Timoshenko beam, the exact equilibrium model developed in §5.6 of Przemieniecki[7] is matched by $\beta = \beta_{C0} = 1/(1+\phi)$, $\phi = 12EI_z/(GA_sL^2)$, in which $A_s = 5bh/6$ is the shear area and $G = \frac{1}{2}E/(1+\nu)$ the shear modulus. The morphed β_m is always higher than β_{C0} for all $0 \le \nu \le \frac{1}{2}$ and aspect ratios $\gamma > 0$. This indicates that in beam-like problems involving transverse shear the rectangular panel will be stiffer than the exact C^0 beam model. For example if $\nu = 1/4$

$$\frac{\beta_{C0}}{\beta_m} = \frac{5}{2(3+\gamma^2)}. \tag{49}$$

This never exceeds 5/6 and goes to zero as $\gamma \to \infty$. This reflects the fact that a 4-node panel can only respond to such antisymmetric nodal motions by deforming in pure shear. The symmetric response, however, is exact for any aspect ratio γ, confirming the optimality of StressRP (= BORP). Observe also that what was a higher order patch test on the two-triangle mesh unit becomes a basic (constant-moment) patch test on the morphed element. This is typical of morphing transformations that reduce spatial dimensionality.

For nonoptimal elements, one finds that the basic stiffness of the morphed beam is wrong except under very special circumstances. For example isotropic StrainRP with zero ν, or one of the SRI elements studied next.

10 A G3 DEVICE: SELECTIVE REDUCED INTEGRATION

The three canonical models of Sections 4-6 were known by the end of Generation 2. Next a third generation tool will be studied in the context of templates. Full Reduced Integration (FRI) and Selective Reduced Integration (SRI) emerged during 1969–72[84–87] as tools to "unlock" isoparametric displacement models. Initially labeled as "variational crimes" by Strang[33] they were eventually justified through lawful association with mixed variational methods.[88–90] Both FRI and SRI turned out to be particularly useful for legacy and nonlinear codes because they allow shape function and numerical integration modules to be reused. For the 4-node panel only SRI is considered because FRI leads to rank deficiency: $R_{11} = R_{12} = R_{22} = 0$. Two questions can be posed:

(i) Can the template (31)–(32) be reproduced for any material law by a SRI scheme?

(ii) Can BORP be cloned for any material law by a SRI scheme that is independent of the aspect ratio?

As shown below, the answers are (i): yes if $R_{12} = 0$; (ii): yes.

10.1 Concept and Notation

In the FEM literature, SRI identifies a scheme for forming $\mathbf{K}$ as the sum of two or more matrices computed with different integration rules and different constitutive properties, within the framework of the isoparametric (iso-P) displacement model. We will focus here on a two-way constitutive decomposition. Split the plane stress constitutive matrix $\mathbf{E}$ into

$$\mathbf{E} = \mathbf{E}_{\rm I} + \mathbf{E}_{\rm II}. \tag{50}$$

The iso-P displacement formulation leads to the expression $\mathbf{K} = \int_{A^e} h\,\mathbf{B}_u^T\mathbf{E}\,\mathbf{B}_u\,d\Omega$ where A^e is the element area and $\mathbf{B}_u$ the iso-P strain-displacement matrix. To apply SRI

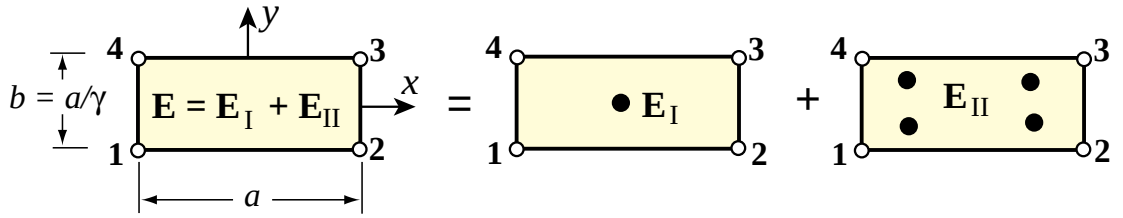

Figure 11. Matrix split for two-way SRI.

insert the splitting (50) into **E** to get two integrals:

$$\mathbf{K} = \int_{A^e} h\, \mathbf{B}_u^T \mathbf{E}_{\rm I}\, \mathbf{B}_u\, d\Omega + \int_{A^e} h\, \mathbf{B}_u^T \mathbf{E}_{\rm II}\, \mathbf{B}_u\, d\Omega = \mathbf{K}_{\rm I} + \mathbf{K}_{\rm II}. \tag{51}$$

The two matrices in (51) are done through different numerical quadrature schemes: rule (I) for the first integral and rule (II) for the second. For the rectangular panel the isoparametric model is the 4-node bilinear element. Rules (I) and (II) will be the 1×1 (one point) and 2×2 (4-point) Gauss product rules, respectively. A general split of the elasticity matrix is

$$\mathbf{E} = \mathbf{E}_{\rm I} + \mathbf{E}_{\rm II} = \begin{bmatrix} E_{11}\,\rho_1 & E_{12}\rho_3 & E_{13}\tau_2 \\ E_{12}\,\rho_3 & E_{22}\,\rho_2 & E_{23}\tau_2 \\ E_{13}\,\tau_2 & E_{23}\,\tau_2 & E_{33}\tau_1 \end{bmatrix} + \begin{bmatrix} E_{11}(1-\rho_1) & E_{12}(1-\rho_3) & E_{13}(1-\tau_2) \\ E_{12}(1-\rho_3) & E_{22}(1-\rho_2) & E_{23}(1-\tau_3) \\ E_{13}(1-\tau_2) & E_{23}(1-\tau_3) & E_{33}(1-\tau_1) \end{bmatrix}, \tag{52}$$

in which ρ_1, ρ_2, ρ_3, τ_1, τ_2 and τ_3 are dimensionless coefficients to be chosen.

10.2 The Case $R_{12} = 0$

A template with $R_{12} = 0$ and arbitrary $\{R_{11}, R_{22}\}$ is matched by taking

$$\rho_1 = \frac{1-3R_{11}}{E_{11}}, \quad \rho_2 = \frac{1-3R_{22}}{E_{22}}, \quad \tau_1 = \tau_2 = \tau_3 = 1. \tag{53}$$

Since ρ_3 does not appear, it is convenient to set it to one to get a diagonal $\mathbf{E}_{\rm II}$. The resulting split is

$$\mathbf{E}_{\rm I} + \mathbf{E}_{\rm II} = \begin{bmatrix} E_{11}-3R_{11} & E_{12} & E_{13} \\ E_{12} & E_{22}-3R_{22} & E_{23} \\ E_{13} & E_{23} & E_{33} \end{bmatrix} + \begin{bmatrix} 3R_{11} & 0 & 0 \\ 0 & 3R_{22} & 0 \\ 0 & 0 & 0 \end{bmatrix}, \tag{54}$$

To get the optimal element (BORP) set $R_{11} = \frac{1}{3}C_{11}^{-1}$ and $R_{22} = \frac{1}{3}C_{22}^{-1}$:

$$\mathbf{E}_{\rm I} + \mathbf{E}_{\rm II} = \begin{bmatrix} E_{11}-C_{11}^{-1} & E_{12} & E_{13} \\ E_{12} & E_{22}-C_{22}^{-1} & E_{23} \\ E_{13} & E_{23} & E_{33} \end{bmatrix} + \begin{bmatrix} C_{11}^{-1} & 0 & 0 \\ 0 & C_{22}^{-1} & 0 \\ 0 & 0 & 0 \end{bmatrix}, \tag{55}$$

For isotropic material this becomes

$$\mathbf{E}_{\rm I} + \mathbf{E}_{\rm II} = \frac{E}{1-\nu^2}\begin{bmatrix} \nu^2 & \nu & 0 \\ \nu & \nu^2 & 0 \\ 0 & 0 & \frac{1}{2}(1-\nu) \end{bmatrix} + E\begin{bmatrix} 1 & 0 & 0 \\ 0 & 1 & 0 \\ 0 & 0 & 0 \end{bmatrix}. \tag{56}$$

To match the (suboptimal) StrainRP, in which $R_{11} = \frac{1}{3}E_{11}$ and $R_{22} = \frac{1}{3}E_{22}$ the appropriate split is

$$\mathbf{E}_{\rm I} + \mathbf{E}_{\rm II} = \begin{bmatrix} 0 & E_{12} & E_{13} \\ E_{12} & 0 & E_{23} \\ E_{13} & E_{23} & E_{33} \end{bmatrix} + \begin{bmatrix} E_{11} & 0 & 0 \\ 0 & E_{22} & 0 \\ 0 & 0 & 0 \end{bmatrix}. \tag{57}$$

For isotropic material this becomes

$$\mathbf{E}_{\rm I} + \mathbf{E}_{\rm II} = E \begin{bmatrix} 0 & \nu & 0 \\ \nu & 0 & 0 \\ 0 & 0 & \frac{1}{2}(1-\nu) \end{bmatrix} + E \begin{bmatrix} 1 & 0 & 0 \\ 0 & 1 & 0 \\ 0 & 0 & 0 \end{bmatrix}. \tag{58}$$

Some FEM books suggest using the dilatational (a.k.a. volumetric, bulk) elasticity law for $\mathbf{E}_I$. As can be seen, the recommendation is incorrect for this element.

10.3 The Case $R_{12} \neq 0$

The case $R_{12} \neq 0$ arises in anisotropic displacement models in which $E_{13} \neq 0$ and/or $E_{23} \neq 0$. Now τ_2 and τ_3 must verify $E_{13}\gamma^{-1}\tau_2 + E_{23}\gamma\tau_3 = E_{13}\gamma^{-1} + E_{23}\gamma - 3R_{12}$. Solve for that τ_i ($i = 2, 3$) that has an associated nonzero modulus. Note that the aspect ratio γ will generally appear in the SRI rule.

This case lacks practical interest because optimality can be achieved with $R_{12} = 0$. But for DispRP an obvious solution that eliminates all aspect ratio dependent is $\rho_1 = \rho_2 = \rho_3 = \tau_1 = \tau_2 = \tau_3 = 0$, whence $\mathbf{E}_{\rm I} = \mathbf{0}$, $\mathbf{E}_{\rm II} = \mathbf{E}$ and the fully integrated isoP element, which locks, is recovered.

10.4 Selective Directional Integration

The template can also be generated by non-Gaussian rules. For example, the following three-way directional split

$$\mathbf{E}_{\rm I}+\mathbf{E}_{\rm II}+\mathbf{E}_{\rm III} = \begin{bmatrix} E_{11}-C_{11}^{-1} & E_{12} & E_{13} \\ E_{12} & E_{22}-C_{22}^{-1} & E_{23} \\ E_{13} & E_{23} & E_{33} \end{bmatrix} + \begin{bmatrix} C_{11}^{-1} & 0 & 0 \\ 0 & 0 & 0 \\ 0 & 0 & 0 \end{bmatrix} + \begin{bmatrix} 0 & 0 & 0 \\ 0 & C_{22}^{-1} & 0 \\ 0 & 0 & 0 \end{bmatrix}, \tag{59}$$

generates the optimal panel in conjunction with three rules. Rule (I) is one-point Gauss with $\{\xi, \eta\} = \{0, 0\}$ and weight 4; Rule (II) has two points on the $y = 0$ median: $\{\xi, \eta\} = \{0, \pm 1/\sqrt{3}\}$ with weight 2; rule (III) has two points on the $x = 0$ median: $\{\xi, \eta\} = \{\pm 1/\sqrt{3}, 0\}$ with weight 2. This selective directional integration is difficult to extend to arbitrary quadrilaterals while preserving observer invariance.

11 FUTILE FAMILIES

Families are template subsets that arise naturally from specific methods as function of discrete or continuous decision parameters. To render the concept more concrete two historically important, albeit practically useless, families for the rectangular panel are considered next.

11.1 Equilibrium Stress Hybrids

This family was studied in the late 1960s by hapless authors with the not unreasonable belief that "more is better." It is obtained by generalizing the 5-parameter stress form of Section 4 with a polynomial series in $\{x, y\}$. An obvious choice is to make σ_{xx}, σ_{yy} and σ_{xy} complete polynomials in $\{x, y\}$:

$$\sigma_{xx} = \sum_{i,j} a_{ij}\, x^i y^j,\ \ \sigma_{yy} = \sum_{i,j} b_{ij}\, x^i y^j,\ \ \sigma_{xy} = \sum_{i,j} c_{ij}\, x^i y^j,\ \ i \geq 0,\ \ j \geq 0,\ \ i + j \leq n. \tag{60}$$

For a complete expansion of order $n \geq 0$ one gets $3(n+1)(n+2)/2$ coefficients. Imposing strongly the two internal equilibrium equations $(1)_3$ for zero body forces reduces the set to $n_\sigma = 3 + 3n + n^2$ independent coefficients. For $n = 0, 1, 3, 5$ and 7 this gives $n_\sigma = 3, 7, 13, 21$ and 31 coefficients, respectively. (Only odd n is of interest beyond

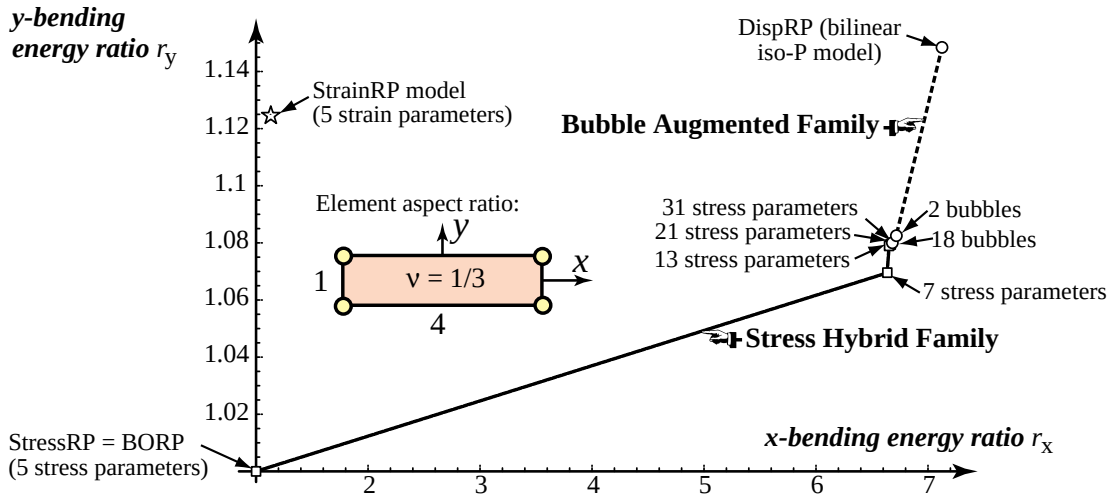

Figure 12. Representation of template families on the $\{r_x, r_y\}$ plane.

$n = 0$, since terms with $i + j = 2, 4, \ldots$ etc., cancel out on integrating strains over the rectangle and have no effect on the element stiffness.)

The stiffness equations of this family can be obtained by the hybrid stress method of Pian and Tong.[28,49] To display the effect of n_σ, the signature of the template (31)–(32) and the associated bending energy ratios were calculated for aspect ratio $\gamma = a/b = 4$, isotropic material with modulus E and Poisson's ratio $\nu = 1/3$.

Table 2. Signatures and Bending Ratios for Stress Hybrid Family

n_σ	5	7	13	21	31
R_{11}/E	0.33333	2.21173	2.21762	2.22125	2.22235
R_{22}/E	0.33333	0.35650	0.35967	0.35979	0.35981
R_{12}	0	0	0	0	0
r_x	1.00000	6.63518	6.65386	6.66375	6.66705
r_y	1.00000	1.06949	1.07900	1.07938	1.07944

The results are collected in Table 2. The bending energy ratios are displayed in Figure 12. Increasing the number of stress terms rapidly stiffens the element in x-bending. This is an instance of what may be called *equilibrium stress futility*: adding more stress terms makes things worse. (The phenomenon is well known but a representation such as that in Figure 12 is new.) As $n_\sigma \to \infty$ the template signature approaches the limit $R_{11}/E \approx 0.2224$ and $R_{22}/E \approx 0.3599$ to 4 places.

11.2 Bubble-Augmented Isoparametrics

A second family can be generated by starting from the conforming iso-P element DispRP of Section 6, and injecting n_b displacement bubble functions. [Bubble are shape functions that vanish over the element boundaries.] The idea is also a late-G2 curiosity but has resurfaced recently. Results for 2 and 18 bubbles (associated with 1 and 9 internal nodes, respectively) are collected in Table 3 and displayed also in Figure 12.

As can be expected injecting bubbles makes the element more flexible but the improvement is marginal. If $n_b \to \infty$ the signature approaches that of the $n_\sigma \to \infty$ hybrid-stress model of the previous subsection. For all this extra work (these models rapidly become expensive on account of high order Gauss integration rules and DOF condensation), r_x decreases from 7.12 to 6.67. This is a convincing illustration of *bubble futility*.

Table 3. Signatures and Bending Ratios for Bubble-Augmented Family

n_b	0	2	18
R_{11}/E	2.37501	2.23894	2.22546
R_{22}/E	0.38281	0.36088	0.35998
R_{12}	0.	0.	0
r_x	7.12505	6.71683	6.67637
r_y	1.14844	1.08265	1.07994

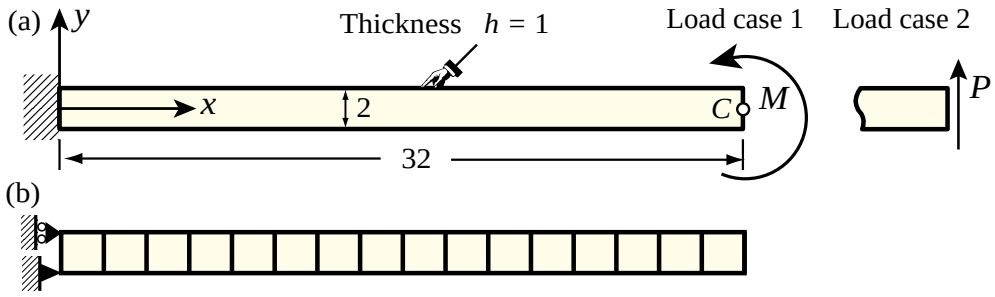

Figure 13. Slender cantilever beam for Examples 1 and 2.
A 16×1 FEM mesh with $\gamma = 1$ is shown in (b).

Figure 12 also marks the energy ratios of the StrainRP element. For this instance $R_{11}/E = R_{22}/E = 3/8 = 0.375$ and $r_x = r_y = 1.125$. Consequently the element is only slightly overstiff. Increasing the number of strain terms, however, would lead to another "futile family."

12 NUMERICAL EXAMPLES

Three benchmark examples involving cantilever beams are studied below. The sequel[3] presents benchmarks involving general quadrilateral shapes and thin-wall shell structures.

12.1 Example 1: Slender Isotropic Cantilever

The slender 16:1 cantilever beam of Figure 13(a) is fabricated of isotropic material, with $E = 7680$, $\nu = 1/4$ and $G = (2/5)E = 3072$. The dimensions are shown in the Figure. Two end load cases are considered: an end moment $M = 1000$ and a transverse end shear $P = 48000/1027 = 46.7381$. Both tip deflections $\delta_C = u_{yC}$ from beam theory: $ML^2/(2EI_z)$ and $PL^3/(3EI_z) + PL/(GA_s)$, in which $I_z = b^3h/12$ and $A_s = 5A/6 = 5bh/6$, are exactly 100. For the second load case the shear deflection is only 0.293% of u_{yC}; thus the particular expression used for A_s is not very important.

Regular meshes with only one element ($N_y = 1$) through the beam height are considered. The number N_x of elements along the span is varied from 1 to 64, giving elements with aspect ratios from $\gamma = 16$ through $\gamma = \frac{1}{4}$. The root clamping condition is imposed by setting u_x to zero at both root nodes, but u_y is only fixed at the lower one thus allowing for Poisson's contraction at the root.

Tables 4 and 5 report computed tip deflections u_{yC} for several element types. The first three rows list results for the 3 rectangular panel models of Sections 4–6. The last three rows give results for selected triangular elements. BODT is the Bending Optimal Drilling Triangle: a 3-node membrane element with drilling freedoms studied in previous papers.[52,81,91,92] ALL-EX is the exactly integrated 1988 Allman triangle with drilling freedoms.[93] CST is the Constant Strain Triangle, also called linear triangle and Turner triangle.[1] Both ALL-EX and BODT have three freedoms per node whereas all others

have two. To get exactly 100.00% from BODT under an end-moment requires particular attention to the end load consistent lumping.[92]

BORP is exact for all γ under end-moment and converges rapidly under end-shear. The performance of BODT is similar, inasmuch as this triangle is constructed to be bending exact in rectangular-mesh units. (In the end-shear load case BORP and BODT, which morph to different beam templates, converge to slightly different limits as $\gamma \to 0$.) StrainRP is about 6% stiffer than BORP, which can be expected since $1/(1-\nu^2) = 16/15$. DispRP, as well as the triangles ALL-EX and CST, lock as γ increases.

The response for more element layers through the height can be readily estimated from equation (45). Consequently those results are omitted to save space. For example, to predict the DispRP answer on a 8×4 mesh under end-moment, proceed as follows. The aspect ratio is $\gamma = 8$. From the $\gamma = 8$ column of Table 4 read off $r_x = 100/3.75 = 26.667$. Set $n = 2$ in (45) to get $r_x^{(4)} = (15 + r_x)/16 = 2.60417$. The estimated tip deflection is $100/2.60417 = 38.40$. Running the program gives $\delta_C = 38.3913$ as average of the y displacement of the two end nodes. Predictions for the end-shear-load case will be less accurate but sufficient for quick estimation.

12.2 Example 2: Slender Anisotropic Cantilever

Next assume that the beam of Figure 13(a) is fabricated of anisotropic material with the elasticity properties

$$\mathbf{E} = \begin{bmatrix} 880 & 600 & 250 \\ 600 & 420 & 150 \\ 250 & 150 & 480 \end{bmatrix}, \quad \mathbf{C} = \mathbf{E}^{-1} = \frac{1}{35580}\begin{bmatrix} 1791 & -2505 & -150 \\ -2505 & 3599 & 180 \\ -150 & 180 & 96 \end{bmatrix}. \tag{61}$$

That these are physically realizable can be checked by getting the eigenvalues of $\mathbf{E}$: {1386.1, 387.3, 6.63}, whence both $\mathbf{E}$ and $\mathbf{C}$ are positive definite. The load magnitudes are adjusted to get beam-theory tip deflections of 100: $M = 2.58672$ and $P = 0.121153$. Since

$$E_{11}C_{11} = 44.297 \tag{62}$$

the energy ratio analysis of Sections 8.3–8.4, through equations (42) and (43), predicts that the strain and displacement models will be big losers, because $r_x \geq 44.297$. This is verified in Tables 6 and 7, which report computed tip deflections u_{yC} for the three rectangular panel models. While BORP shines, the strain and displacement models are way off, regardless of how many elements one puts along x.

Putting more element layers through the height will help StrainRP and DispRP but too slowly to be practical. To give an example, a 128×8 mesh of StrainRP (or clones) under end moment will have $r_x^{(8)} = (63 + 44.297)/64 = 1.676$ and estimated deflection of $100/1.676 = 59.647$. Running that mesh gives $u_{yC} = 59.65$. So using over 2000 freedoms in this fairly trivial problem the results are still off by about 40%.

12.3 Example 3: Short Cantilever Under End Shear

The shear-loaded cantilever beam defined in Figure 14 has been selected as a test problem for plane stress elements by many investigators since proposed in the writer's thesis.[94] A full root-clamping condition is implemented by constraining both displacement components to zero at nodes located on at the root section $x = 0$. The applied shear load varies parabolically over the end section and is consistently lumped at the nodes. The main comparison value is the tip deflection $\delta_C = u_{yC}$ at the center of the end cross section. Reference[81] recommends $\delta_C = 0.35601$, which is also adopted here. The converged value of digits 4-5 is clouded by the mild singularity developing at the root section. This singularity is displayed for σ_{xy} in the form of an intensity contour plot in Figure 15.

Table 4 Tip Deflections (exact=100) for Slender Isotropic Cantilever under End Moment

Element	Mesh: x-subdivisions $\times$ y-subdivisions ($N_x \times N_y$)						
	1×1 ($\gamma = 16$)	2×1 ($\gamma = 8$)	4×1 ($\gamma = 4$)	8×1 ($\gamma = 2$)	16×1 ($\gamma = 1$)	32×1 ($\gamma = \frac{1}{2}$)	64×1 ($\gamma = \frac{1}{4}$)
StressRP (BORP)	100.00	100.00	100.00	100.00	100.00	100.00	100.00
StrainRP	93.75	93.75	93.75	93.75	93.75	93.75	93.75
DispRP	0.97	3.75	13.39	37.49	68.18	85.71	91.60
ALL-EX	0.04	0.63	7.40	35.83	58.44	64.89	66.45
CST	0.32	1.25	4.46	12.50	22.73	28.57	30.53
BODT	100.00	100.00	100.00	100.00	100.00	100.00	100.00

Table 5 Tip Deflections (exact=100) for Slender Isotropic Cantilever under End Shear

Element	Mesh: x-subdivisions $\times$ y-subdivisions ($N_x \times N_y$)						
	1×1 ($\gamma = 16$)	2×1 ($\gamma = 8$)	4×1 ($\gamma = 4$)	8×1 ($\gamma = 2$)	16×1 ($\gamma = 1$)	32×1 ($\gamma = \frac{1}{2}$)	64×1 ($\gamma = \frac{1}{4}$)
StressRP (BORP)	75.02	93.72	98.39	99.56	99.86	99.94	99.97
StrainRP	70.35	87.88	92.26	93.35	93.63	93.71	93.73
DispRP	0.97	3.75	13.39	37.49	68.16	85.69	91.58
ALL-EX	0.24	0.69	6.36	35.18	59.59	65.70	67.03
CST	0.48	1.41	4.62	12.66	22.88	28.73	30.69
BODT	75.20	93.37	98.20	99.55	99.93	100.12	100.15

Table 6 Tip Deflections (exact=100) for Slender Anisotropic Cantilever under End Moment

Element	Mesh: x-subdivisions $\times$ y-subdivisions ($N_x \times N_y$)						
	1×1 ($\gamma = 16$)	2×1 ($\gamma = 8$)	4×1 ($\gamma = 4$)	8×1 ($\gamma = 2$)	16×1 ($\gamma = 1$)	32×1 ($\gamma = \frac{1}{2}$)	64×1 ($\gamma = \frac{1}{4}$)
StressRP (BORP)	100.00	100.00	100.00	100.00	100.00	100.00	100.00
StrainRP	2.26	2.26	2.26	2.26	2.26	2.26	2.26
DispRP	0.02	0.07	0.25	0.76	1.53	2.08	2.25

Table 7 Tip Deflections (exact=100) for Slender Anisotropic Cantilever under End Shear

Element	Mesh: x-subdivisions $\times$ y-subdivisions ($N_x \times N_y$)						
	1×1 ($\gamma = 16$)	2×1 ($\gamma = 8$)	4×1 ($\gamma = 4$)	8×1 ($\gamma = 2$)	16×1 ($\gamma = 1$)	32×1 ($\gamma = \frac{1}{2}$)	64×1 ($\gamma = \frac{1}{4}$)
StressRP (BORP)	74.95	93.68	98.37	99.54	99.84	99.92	99.96
StrainRP	1.70	2.12	2.22	2.26	2.26	2.26	2.26
DispRP	0.02	0.07	0.25	0.75	1.52	2.06	2.23

Table 8 gives computed deflections for rectangular mesh units with aspect ratios of 1, 2 and 4, using the three canonical rectangular panel models and the three triangles identified in Example 1. For end deflection reporting the load was scaled by $(100/0.35601)$ so that the "theoretical solution" becomes 100.00. (In comparing stress values the unscaled load of $P = 40$ was used.) There are no drastically small deflections because element aspect

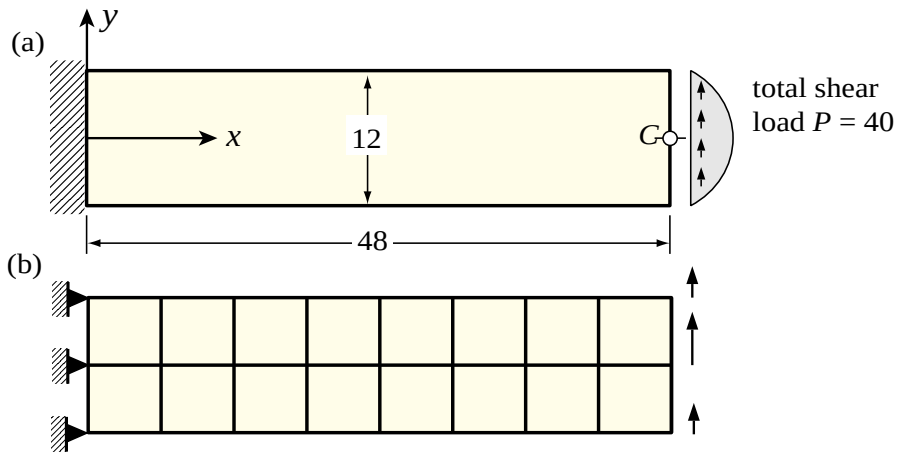

Figure 14. Short cantilever under end-shear benchmark: $E = 30000$, $\nu = 1/4$, $h = 1$; root contraction not allowed, a 8×2 mesh is shown in (b).

Figure 15. Intensity contour plot of σ_{xy} given by the 64×16 BORP mesh. Produced by *Mathematica* and Gaussian filtered by Adobe Photoshop. Stress node values averaged between adjacent elements. The root singularity pattern is clearly visible.

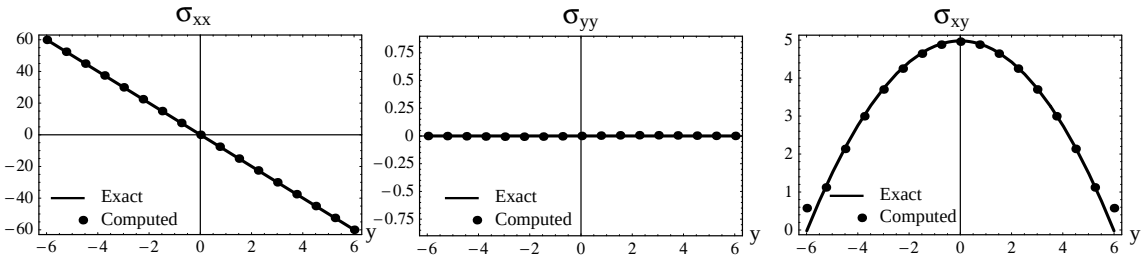

Figure 16. Distributions of σ_{xx}, σ_{yy} and σ_{xy} at $x = 12$ given by the 64×16 BORP mesh. Stress node values averaged between adjacent elements. Note different stress scales. Deviations at $y = \pm 6$ (free edges) due to "upwinded" y averaging.

ratios only go up to 4:1. Elements StressRP (BORP), StrainRP and BODT outperformed the others. There is little to choose between these 3 models, which is typical of isotropic materials. The BODT triangle is more versatile but carries one more freedom per node.

Figure 16 plots averaged node stress values at section $x = 12$ computed from the 64×16 BORP mesh. The agreement with the standard beam stress distribution (that section being sufficiently away from the root) is very good except for σ_{xy} near the free edges $y = \pm 6$, at which the interelement averaging process becomes biased.

13 DISCUSSION AND CONCLUSIONS

What can templates contribute to FEM technology? Advantages in two areas are clear:

Synthesis. Only one procedure (module, function, subroutine) is written to do many elements. This simplifies comparison and verification benchmarking, as well as streamlining

Table 8 Tip Deflections (exact = 100) for Short Cantilever under End Shear

Element	Mesh: x-subdivisions $\times$ y-subdivisions ($N_x \times N_y$)				
	8×2	16×4	32×8	64×16	128×32
StressRP (BORP)	98.80	99.59	99.88	99.97	100.00
StrainRP	97.24	99.19	99.77	99.94	99.99
DispRP	88.83	96.83	99.16	99.78	99.95
ALL-EX	89.43	96.88	99.16	99.79	99.96
CST	55.09	82.59	94.90	98.65	99.66
BODT	101.68	100.30	100.03	100.00	100.00
	4×2	8×4	16×8	32×16	64×32
StressRP (BORP)	97.22	99.08	99.71	99.92	99.99
StrainRP	95.67	98.67	99.61	99.89	99.98
DispRP	69.88	90.05	97.24	99.28	99.82
ALL-EX	70.71	89.63	96.93	99.15	99.77
CST	37.85	69.86	90.04	97.25	99.28
BODT	96.68	98.44	99.37	99.78	99.93
	2×2	4×4	8×8	16×16	32×32
StressRP (BORP)	91.94	97.41	99.19	99.75	99.93
StrainRP	90.47	97.03	99.07	99.72	99.92
DispRP	37.84	70.57	90.39	97.35	99.31
ALL-EX	26.16	56.93	83.54	95.14	98.69
CST	17.83	43.84	75.01	92.13	97.86
BODT	92.24	96.99	98.70	99.48	99.81

maintenance. A unified implementation automatically weeds out clones.

Customability. Templates can produce optimal and custom elements not obtainable (or hard to obtain) through conventional methods.

A striking example of the latter is the UBOTP macroelement presented in Section A.3 of the Appendix. This concludes a three decade search for a four noded trapezoid which is insensitive to distortion, passes the patch test and retains rank sufficiency. To the writer's knowledge, this model, as well as its generalization to an arbitrary quadrilateral presented in the sequel[3] cannot be obtained with conventional formulations.

Will the synthesis power translate into teaching changes in finite element courses? This is not presently likely. Two reasons can be cited.

First, advantages may show up only in advanced or seminar-level courses. Beginning calculus students are not taught Lebesgue integration and distribution theory despite their wider scope. Likewise, introductory FEM courses are best organized around a few specific methods. Students must be exposed to a range of formulations and hands-on work before they can appreciate the advantages of unified implementation.

Second, the theory has not progressed to the point where the configuration of a template can be written down from first principles in front of an audience. Only two general rules are presently known: the fundamental decomposition into basic and higher order components, and the procedure to get the matrix structure of the basic component. No general rules to construct the higher order component can be stated aside from orthogonality and definiteness constraints.

How far can templates go? As of this writing templates are only known for a few elements in one and two dimensions, such as beams and flat plates of simple geometry. What is the major technical obstacle to go beyond those? Symbolic power. One must rely on computer-aided symbolic manipulation because geometric, constitutive and fabrication

properties must be carried along as variables. This can lead, and does, to a combinatorial tarpit as elements become more complicated.

The good news is that computer algebra programs are gradually becoming more powerful, and are now routinely available on laptops and personal computers. Over the next 5 years PCs are expected to migrate to 64-bit multiple-CPUs capable of addressing hundreds of GBs of memory at over 10GHz cycle speeds. As that happens the development of templates for 3D solid and shell elements in reasonable time will become possible.

Acknowledgements

Preparation of this paper has been supported by the National Science Foundation under Grant CMS–0219422, by the Finite Elements for Salinas contract with Sandia National Laboratories, and by a faculty fellowship from the Ministerio de Educación y Cultura de España to visit the Centro Internacional de Métodos Numéricos en Ingenería (CIMNE) in Barcelona from April to July 2002.

References

[1] M. J. Turner, R. W. Clough, H. C. Martin and L. J. Topp, Stiffness and deflection analysis of complex structures, *J. Aero. Sci.*, **23**, 805–824 (1956).

[2] R. H. MacNeal, A theorem regarding the locking of tapered four noded membrane elements, *Int. J. Numer. Meth. Engrg.*, **24**, 1793–1799 (1987).

[3] C. A. Felippa, A 4-noded quadrilateral that sidesteps MacNeal's theorem, in preparation.

[4] C. A. Felippa, A historical outline of matrix structural analysis: a play in three acts, *Computers & Structures*, **79**, 1313–1324 (2001).

[5] J. H. Argyris and S. Kelsey, *Energy Theorems and Structural Analysis*, London, Butterworth (1960). Part I reprinted from *Aircr. Engrg.*, **26**, Oct-Nov 1954 and **27**, April-May 1955.

[6] E. C. Pestel and F. A. Leckie, *Matrix Methods in Elastomechanics*, McGraw-Hill, New York, (1963).

[7] J. S. Przemieniecki, *Theory of Matrix Structural Analysis*, McGraw-Hill, New York (1968). Dover edition (1986).

[8] R. H. Gallaguer, *A Correlation Study of Methods of Matrix Structural Analysis*, Pergamon, Oxford (1964).

[9] R. F. Melosh, Bases for the derivation of matrices for the direct stiffness method, *AIAA J.*, **1**, 1631–1637 (1963).

[10] M. J. Turner, The direct stiffness method of structural analysis, Structural and Materials Panel Paper, AGARD Meeting, Aachen, Germany (1959).

[11] M. J. Turner, E. H. Dill, H. C. Martin and R. J. Melosh, Large deflection analysis of complex structures subjected to heating and external loads, *J. Aero. Sci.*, **27**, pp. 97-107 (1960).

[12] M. J. Turner, H. C. Martin and R. C. Weikel, Further development and applications of the stiffness method, in *AGARDograph 72: Matrix Methods of Structural Analysis*, ed. by B. M. Fraeijs de Veubeke, Pergamon Press, New York, 203–266 (1964).

[13] R. F. Melosh, Development of the stiffness method to define bounds on the elastic behavior of structures, *Ph.D. Dissertation*, University of Washington, Seattle (1962).

[14] B. M. Fraeijs de Veubeke, Upper and lower bounds in matrix structural analysis, in *AGARDograph 72: Matrix Methods of Structural Analysis*, ed. by B. M. Fraeijs de Veubeke, Pergamon Press, New York, 174–265 (1964).

[15] R. W. Clough, The finite element method – a personal view of its original formulation, in *From Finite Elements to the Troll Platform – the Ivar Holand 70th Anniversary Volume*, ed. by K. Bell, Tapir, Norway, 89–100 (1994).

[16] R. W. Clough, The finite element method in plane stress analysis, *Proc. 2nd ASCE Conf. on Electronic Computation*, Pittsburgh, Pa (1960).

[17] R. W. Clough, The finite element method in structural mechanics, in *Stress Analysis*, ed. by O. C. Zienkiewicz and G. S. Holister, Wiley, London, 85–119 (1965).

[18] B. M. Fraeijs de Veubeke, Displacement and equilibrium models, in *Stress Analysis*, ed. by O. C. Zienkiewicz and G. Hollister, Wiley, London, 145–197, 1965; reprinted in *Int. J. Numer. Meth. Engrg.*, **52**, 287–342 (2001).

[19] O. C. Zienkiewicz and Y. K. Cheung, *The Finite Element Method in Engineering Science*, McGraw-Hill, London (1967).

[20] O. C. Zienkiewicz and Y. K. Cheung, Finite elements in the solution of field problems, *The Engineer*, 507–510 (1965).

[21] B. M. Irons, Engineering application of numerical integration in stiffness methods, *AIAA J.*, **4**, pp. 2035–2037 (1966).

[22] B. M. Irons and J. Barlow, Comments on 'matrices for the direct stiffness method' by R. J. Melosh, *AIAA J.*, **2**, 403 (1964).

[23] G.P. Bazeley, Y. K. Cheung, B. M. Irons and O. C. Zienkiewicz, Triangular elements in plate bending – conforming and nonconforming solutions, in *Proc. 1st Conf. Matrix Meth. Struc. Mech.*, ed. by J. Przemieniecki et. al., AFFDL-TR-66-80, Air Force Institute of Technology, Dayton, Ohio, 547–576 (1966).

[24] J. Ergatoudis, B. M. Irons and O. C. Zienkiewicz, Curved, isoparametric, "quadrilateral" elements for finite element analysis, *Int. J. Solids Struc.*, **4**, 31–42 (1968).

[25] B. M. Irons and S. Ahmad, *Techniques of Finite Elements*, Ellis Horwood Ltd, Chichester, UK (1980).

[26] T. H. H. Pian, Derivation of element stiffness matrices by assumed stress distributions, *AIAA J.*, **2**, 1333–1336 (1964).

[27] T. H. H. Pian, Element stiffness matrices for boundary compatibility and for prescribed boundary stresses, in *Proc. 1st Conf. on Matrix Methods in Structural Mechanics*, AFFDL-TR-66-80, Air Force Institute of Technology, Dayton, Ohio, 457–478 (1966).

[28] T. H. H. Pian and P. Tong, Basis of finite element methods for solid continua, *Int. J. Numer. Meth. Engrg.*, **1**, 3–29 (1969).

[29] T. H. H. Pian, Some notes on the early history of hybrid stress finite element method, *Int. J. Numer. Meth. Engrg.*, **47**, 419–425 (2000).

[30] L. R. Herrmann, Elasticity equations for nearly incompressible materials by a variational theorem, *AIAA Journal*, **3**, 1896–1900 (1965).

[31] R. L. Taylor, K. S. Pister and L. R. Herrmann, A variational principle for incompressible and nearly incompressible orthotropic elasticity, *Int. J. Solids Struc.*, **4**, 875-883 (1968).

[32] G. Strang and G. Fix, *An Analysis of the Finite Element Method*. Prentice-Hall, (1973).

[33] G. Strang, Variational crimes in the finite element method, in *The Mathematical Foundations of the Finite Element Method with Applications to Partial Differential Equations*, ed. by A. K. Aziz, Academic Press, New York, 689–710 (1972).

[34] T. J. R. Hughes, *The Finite Element Method: Linear Static and Dynamic Finite Element Analysis*, Prentice Hall, Englewood Cliffs, N. J. (1987).

[35] K.-J. Bathe, *Finite Element Procedures in Engineering Analysis*, Prentice Hall, Englewood Cliffs, N. J., 1982.

[36] S. N. Atluri, R. N. Gallagher and O. C. Zienkiewicz, (eds.), *Hybrid and Mixed Finite Element Methods*, Wiley, New York (1983).

[37] R. H. MacNeal, Derivation of element stiffness matrices by assumed strain distribution, *Nuclear Engrg. Design*, **70**, 3–12 (1978)

[38] B. Szabo and I. Babuska, *Finite Element Analysis* Wiley, New York (1991).

[39] R. H. MacNeal, The evolution of lower order plate and shell elements in MSC/NASTRAN, in T. J. R. Hughes and E. Hinton (eds.), *Finite Element Methods for Plate and Shell Structures, Vol. I: Element Technology*, Pineridge Press, Swansea, U.K., 85–127 (1986).

[40] R. H. MacNeal, *Finite Elements: Their Design and Performance*, Marcel Dekker, New York (1994).

[41] P. G. Bergan, Finite elements based on energy orthogonal functions, *Int. J. Numer. Meth. Engrg.*, **15**, 1141–1555 (1980).

[42] P. G. Bergan and M. K. Nygård, Finite elements with increased freedom in choosing shape functions, *Int. J. Numer. Meth. Engrg.*, **20**, 643–664 (1984).

[43] D. P. Flanagan and T. Belytschko, A uniform strain hexahedron and quadrilateral with orthogonal hourglass control, *Int. J. Numer. Meth. Engrg.*, **17**, 679–706 (1981).

[44] K.-J. Bathe and E. N. Dvorkin, A four-node plate bending element based on Mindlin-Reissner plate theory and a mixed interpolation, *Int. J. Numer. Meth. Engrg.*, **21**, 367–383 (1985).

[45] H. C. Huang and E. Hinton, A new nine node degenerated shell element with enhanced membrane and shear interpolation, *Int. J. Numer. Meth. Engrg.*, **22**, 73–92 (1986).

[46] K. C. Park, G. M. Stanley, A curved C^0 shell element based on assumed natural-coordinate strains, *J. Appl. Mech.*, **53**, 278–290 (1986).

[47] G. M. Stanley, K. C. Park and T. J. R. Hughes, Continuum based resultant shell elements, in T. J. R. Hughes and E. Hinton (eds.), *Finite Element Methods for Plate and Shell Structures, Vol. I: Element Technology*, Pineridge Press, Swansea, U.K., 1–45 (1986)

[48] T. H. H. Pian and K. Sumihara, Rational approach for assumed stress finite elements, *Int. J. Numer. Meth. Engrg.*, **20**, 1685–1695 (1984).

[49] T. H. H. Pian and P. Tong, Relations between incompatible displacement model and hybrid stress model, *Int. J. Numer. Meth. Engrg.*, **22**, 173-181 (1986).

[50] E. F. Punch and S. N. Atluri, Development and testing of stable, invariant, isoparametric curvilinear 2- and 3D hybrid stress elements, *Comp. Meths. Appl. Mech. Engrg.*, **47**, 331–356 (1984).

[51] C. Militello and C. A. Felippa, The First ANDES Elements: 9-DOF Plate Bending Triangles, *Comp. Meths. Appl. Mech. Engrg.*, **93**, 217–246 (1991).

[52] C. A. Felippa and C. Militello, Membrane triangles with corner drilling freedoms: II. The ANDES element, *Finite Elements Anal. Des.*, **12**, 189–201 (1992).

[53] J. C. Simo and T. J. R. Hughes, On the variational foundations of assumed strain methods, *J. Appl. Mech.*, **53**, 51–54 (1986).

[54] J. C. Simo and M. S. Rifai, A class of mixed assumed strain methods and the method of incompatible modes, *Int. J. Numer. Meth. Engrg.*, **29**, 1595–1638 (1990).

[55] C. A. Felippa and C. Militello, Developments in variational methods for high performance plate and shell elements, in *Analytical and Computational Models for Shells*, CED Vol. 3, Eds. A. K. Noor, T. Belytschko and J. C. Simo, The American Society of Mechanical Engineers, ASME, New York, 191–216 (1989).

[56] P. G. Bergan and L. Hanssen, A New Approach for Deriving 'Good' Finite Elements, in *The Mathematics of Finite Elements and Applications – Volume II*, ed. by J. R. Whiteman, Academic Press, London, 483–497, (1975).

[57] L. Hanssen, P. G. Bergan and T. J. Syversten, Stiffness derivation based on element convergence requirements, in *The Mathematics of Finite Elements and Applications – Volume III*, ed. by J. R. Whiteman, Academic Press, London, 83–96, (1979).

[58] P. G. Bergan and C. A. Felippa, A triangular membrane element with rotational degrees of freedom, *Comp. Meths. Appl. Mech. Engrg.*, **50**, 25–69 (1985).

[59] B. M. Fraeijs de Veubeke, Diffusive equilibrium models, in M. Geradin (ed.), *B. M. Fraeijs de Veubeke Memorial Volume of Selected Papers*, Sitthoff & Noordhoff, Alphen aan den Rijn, The Netherlands, 569–628 (1980).

[60] P. G. Bergan and C. A. Felippa, Efficient implementation of a triangular membrane element with drilling freedoms, in T. J. R. Hughes and E. Hinton (eds.), *Finite Element Methods for Plate and Shell Structures, Vol. I: Element Technology*, Pineridge Press, Swansea, U.K., 128–152 (1986).

[61] M. K. Nygård, The Free Formulation for nonlinear finite elements with applications to shells, *Ph. D. Dissertation*, Division of Structural Mechanics, NTH, Trondheim, Norway (1986).

[62] C. A. Felippa and P. G. Bergan, A triangular plate bending element based on an energy-orthogonal free formulation, *Comp. Meths. Appl. Mech. Engrg.*, **61**, 129–160 (1987).

[63] C. A. Felippa, Parametrized multifield variational principles in elasticity: II. Hybrid functionals and the free formulation, *Comm. Appl. Numer. Meth.*, **5**, 79–88 (1989).

[64] C. A. Felippa, The extended free formulation of finite elements in linear elasticity, *J. Appl. Mech.*, **56**, 609–616 (1989).

[65] G. Skeie, The Free Formulation: linear theory and extensions with applications to tetrahedral elements with rotational freedoms, *Ph. D. Dissertation*, Division of Structural Mechanics, NTH, Trondheim, Norway (1991).

[66] C. A. Felippa and R. W. Clough, The finite element method in solid mechanics, in *Numerical Solution of Field Problems in Continuum Physics*, ed. by G. Birkhoff and R. S. Varga, SIAM–AMS Proceedings II, American Mathematical Society, Providence, R.I., 210–252 (1969).

[67] I. C. Taig and R. I. Kerr, Some problems in the discrete element representation of aircraft structures, in *Matrix Methods of Structural Analysis*, ed. by B. M. Fraeijs de Veubeke, Pergamon Press, London (1964).

[68] E. L. Wilson, R. L. Taylor, W. P. Doherty and J. Ghaboussi, Incompatible displacement models, in *Numerical and Computer Models in Structural Mechanics*, ed. by S. J. Fenves, N. Perrone, A. R. Robinson and W. C. Schnobrich, Academic Press, New York, 43–57 (1973).

[69] R. L. Taylor, E. L. Wilson and P. J. Beresford, A nonconforming element for stress analysis, *Int. J. Numer. Meth. Engrg.*, **10**, 1211–1219 (1976).

[70] T. Belytschko, W. K. Liu and B. E. Engelmann, The gamma elements and related developments, in T. J. R. Hughes and E. Hinton (eds.), *Finite Element Methods for Plate and Shell Structures, Vol. I: Element Technology*, Pineridge Press, Swansea, U.K., 316–347 (1986).

[71] R. H. MacNeal, A simple quadrilateral shell element, *Computers & Structures*, **8**, 175–183 (1978).

[72] N. Lautersztajn-S and A. Samuelsson, Further discussion on four-node isoparametric elements in plane bending, *Int. J. Numer. Meth. Engrg.*, **47**, 129–140 (2000).

[73] C. A. Felippa, A survey of parametrized variational principles and applications to computational mechanics, *Comp. Meths. Appl. Mech. Engrg.*, **113**, 109–139 (1994).

[74] C. A. Felippa, B. Haugen and C. Militello, From the individual element test to finite element templates: evolution of the patch test, *Int. J. Numer. Meth. Engrg.*, **38**, 199–222 (1995).

[75] C. A. Felippa, Parametrized unification of matrix structural analysis: classical formulation and d-connected mixed elements, *Finite Elements Anal. Des.*, **21**, 45–74 (1995).

[76] C. A. Felippa, Recent developments in parametrized variational principles for mechanics, *Comput. Mech.*, **18**, 159–174, 1996.

[77] C. A. Felippa and C. Militello, Construction of optimal 3-node plate bending elements by templates, *Comput. Mech.*, **24**, 1–13 (1999).

[78] C. A. Felippa, Recent developments in basic finite element technologies, in *Computational Mechanics in Structural Engineering-Recent Developments*, ed. by F.Y. Cheng and Y. Gu, Elsevier, Amsterdam, 141–156, 1999.

[79] C. A. Felippa, Recent advances in finite element templates, in *Computational Mechanics for the Twenty-First Century*, ed. by B.J.V. Topping, Saxe-Coburn Pub., Edinburgh, 71–98, 2000.

[80] C. Militello and C. A. Felippa, The individual element patch revisited, in *The Finite Element Method in the 1990's — a book dedicated to O. C. Zienkiewicz*, ed. by E. Oñate, J. Periaux and A. Samuelsson, CIMNE, Barcelona and Springer-Verlag, Berlin, 554–564 (1991).

[81] C. A. Felippa, A study of optimal membrane triangles with drilling freedoms, *Comp. Meths. Appl. Mech. Engrg.*, **192**, 2125–2168 (2003).

[82] C. A. Felippa, Customizing the mass and geometric stiffness of plane thin beam elements by Fourier methods, *Engrg. Comput.*, **18**, 286–303 (2001).

[83] C. A. Felippa, Customizing high performance elements by Fourier methods, *Trends in Computational Mechanics*, ed. by W. A. Wall, K.-U. Bleitzinger and K. Schweizerhof, CIMNE, Barcelona, Spain, 283-296 (2001).

[84] W. P. Doherty, E. L. Wilson and R. L. Taylor, Stress analysis of axisymmetric solids utilizing higher order quadrilateral finite elements, SESM Report 69-3, Department of Civil Engineering, University of California, Berkeley (1969).

[85] O. C. Zienkiewicz, R. L. Taylor and J. M. Too, Reduced integration technique in general analysis of plates and shells, *Int. J. Numer. Meth. Engrg.*, **3**, 275–290 (1971).

[86] S. F. Pawsey and R. W. Clough, Improved numerical integration of thick shell finite elements, *Int. J. Numer. Meth. Engrg.*, **3**, 545–586 (1971).

[87] K. Kavanagh and S. W. Key, A note on selective and reduced integration techniques in the finite element method, *Int. J. Numer. Meth. Engrg.*, **4**, 148–150 (1972).

[88] T. J. R. Hughes, Generalization of selective integration procedures to anisotropic and nonlinear media, *Int. J. Numer. Meth. Engrg.*, **15**, 1413–148 (1980).

[89] T. J. R. Hughes and D. S. Malkus, Mixed finite element methods – reduced and selective integration techniques: a unification of concepts, *Comp. Meths. Appl. Mech. Engrg.*, bf 15, 63–81 (1978).

[90] T. J. R. Hughes and D. S. Malkus, A general penalty mixed equivalence theorem for anisotropic, incompressible finite elements, in *Hybrids and Mixed Finite Element Methods*, ed. by S. N. Atluri, R. H. Gallagher and O. C. Zienkiewicz, Wiley, London (1983).

[91] K. Alvin, H. M. de la Fuente, B. Haugen and C. A. Felippa, Membrane triangles with corner drilling freedoms: I. The EFF element, *Finite Elements Anal. Des.*, **12**, 163–187 (1992).

[92] C. A. Felippa and S. Alexander, Membrane triangles with corner drilling freedoms: III. Implementation and performance evaluation, *Finite Elements Anal. Des.*, **12**, 203–239 (1992).

[93] D. J. Allman, Evaluation of the constant strain triangle with drilling rotations, *Int. J. Numer. Meth. Engrg.*, **26**, 2645–2655 (1988).

[94] C. A. Felippa, Refined finite element analysis of linear and nonlinear two-dimensional structures, *Ph.D. Dissertation*, Department of Civil Engineering, University of California at Berkeley, Berkeley, CA (1966).

[95] C. A. Felippa and K. C. Park, Fitting strains and displacements by minimizing dislocation energy, Proceedings of the Sixth International Conference on Computational Structures Technology, Prague, Czech Republic, 49–51 (2002). Complete text in CDROM.

[96] C. A. Felippa and K. C. Park, The construction of free-free flexibility matrices for multilevel structural analysis, *Comp. Meths. Appl. Mech. Engrg.*, **191**, 2111-2140 (2002).

[97] R. H. MacNeal and R. L. Harder, A proposed standard set of problems to test finite element accuracy, *Finite Elements Anal. Des.*, **1**, 3–20 (1985).

[98] C. C. Wu and Y. K. Cheung, On optimization approaches of hybrid stress elements, *Finite Elements Anal. Des.*, **21**, 111–128 (1995).

Appendix A. MORE GENERAL PANEL GEOMETRIES

The template framework of four noded membrane elements can be extended to more general geometries, at the cost of increased complexity in symbolic computations. As an aperitif for the sequel[3] this appendix present templates for parallelogram and trapezoidal geometries.

The first-generation (pre-1962) direct elasticity methods recalled in Sections 4–5 do not work properly beyond the parallelogram. The resulting "node collocation" elements fail the patch test and thus cannot fit in the template framework.

Variational methods are required to get stress-assumed and strain-assumed elements that work. For stress elements the Hellinger-Reissner (HR) principle is used. For strain elements, a strain-fit method[95] in conjunction with de Veubeke's strain-displacement mixed functional is used.

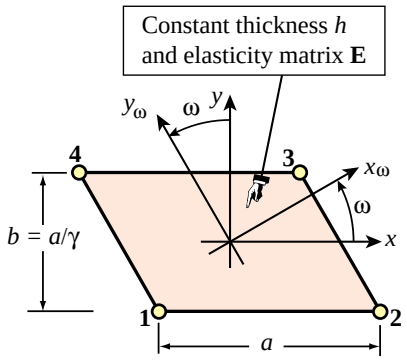

Figure 17. The 4-node swept panel.

A.1 Parallelogram (Swept) Panel

The geometry of the parallelogram panel shown in Figure 17 is defined by the dimensions a, b and the skewangle ω, positive counterclockwise. The template again has the configuration (31) displayed in Figure 6.

With $s = \tan\omega$ the matrices to be adjusted are

$$\mathbf{W} = \begin{bmatrix} \frac{1}{a} & 0 \\ -\frac{s}{b} & \frac{1}{b} \end{bmatrix},$$
$$\mathbf{H}_c = \frac{1}{2ab}\begin{bmatrix} -b & 0 & b & 0 & b & 0 & -b & 0 \\ 0 & -a-bs & 0 & -a+bs & 0 & a+bs & 0 & a-bs \\ -a-bs & -b & -a+bs & b & a+bs & b & a-bs & -b \end{bmatrix}, \tag{63}$$

The higher order projector $\mathbf{H}_h$ is exactly as in (32), whereas $\mathbf{R}$ depends on the formulation, as explained below. For future use the compliance and elasticity along the median direction y_ω (see Figure 17) are denoted by

$$\begin{aligned} C^\omega_{22} &= C_{22}\cos^4\omega - 2C_{23}\cos^3\omega\sin\omega + (2C_{12}{+}C_{33})\cos^2\omega\sin^2\omega - 2C_{13}\cos\omega\sin^3\omega \\ &\quad + C_{11}\sin^4\omega = \frac{C_{22} - 2C_{23}s + (2C_{12}+C_{33})s^2 - 2C_{13}s^3 + C_{11}s^4}{(1+s^2)^2}, \\ E^\omega_{22} &= E_{22}\cos^4\omega - 4E_{23}\cos^3\omega\sin\omega + (2E_{12}{+}4E_{33})\cos^2\omega\sin^2\omega - 4E_{13}\cos\omega\sin^3\omega \\ &\quad + E_{11}\sin^4\omega = \frac{E_{22} - 4E_{23}s + (2E_{12}+4E_{33})s^2 - 4E_{13}s^3 + E_{11}s^4}{(1+s^2)^2}. \end{aligned} \tag{64}$$

Stress element. A 5-parameter stress element StressPP can be constructed either directly, as done by Gallagher[8] or by the HR principle, starting from the energy-orthogonal stress field

$$\begin{bmatrix} \sigma_{xx} \\ \sigma_{yy} \\ \sigma_{xy} \end{bmatrix} = \begin{bmatrix} 1 & 0 & 0 & y/b & \sin^2\omega\, x_\omega \\ 0 & 1 & 0 & 0 & \cos^2\omega\, x_\omega \\ 0 & 0 & 1 & 0 & -\sin\omega\cos\omega\, x_\omega \end{bmatrix} \begin{bmatrix} \mu_1 \\ \mu_2 \\ \mu_3 \\ \mu_4 \\ \mu_5 \end{bmatrix}, \tag{65}$$

in which $\sin\omega = s/\sqrt{1+s^2}$, $\cos\omega = 1/\sqrt{1+s^2}$, and $x_\omega = (x\cos\omega + y\sin\omega)/(a\cos\omega) = (x+ys)/a$. Both methods give the same stiffness. [Because (65) is an equilibrium field, an equilibrium stress hybrid formulation gives the same answer.] The stiffness is matched by the template with

$$R_{11} = \frac{1}{3C_{11}}, \quad R_{12} = 0, \quad R_{22} = \frac{1}{3C^{\omega}_{22}\,(1+s^2)^2}. \tag{66}$$

If the material is isotropic the diagonal entries are $R_{11} = \frac{1}{3}E$ and $R_{22} = \frac{1}{3}E/(1+s^2)^2$. The Q6 and QM6 elements continue to be clones of StressPP.

Strain element. A 5-parameter strain element StrainPP can be constructed by the direct elasticity method of Section 5, or by a variational strain-fitting method[95], starting from the companion of (65):

$$\begin{bmatrix} e_{xx} \\ e_{yy} \\ 2e_{xy} \end{bmatrix} = \begin{bmatrix} 1 & 0 & 0 & y/b & \sin^2\omega\, x_\omega \\ 0 & 1 & 0 & 0 & \cos^2\omega\, x_\omega \\ 0 & 0 & 1 & 0 & -2\sin\omega\cos\omega\, x_\omega \end{bmatrix} \begin{bmatrix} \chi_1 \\ \chi_2 \\ \chi_3 \\ \chi_4 \\ \chi_5 \end{bmatrix}. \tag{67}$$

Both methods give the same result. The stiffness is matched by setting

$$R_{11} = \tfrac{1}{3}E_{11}, \quad R_{12} = 0, \quad R_{22} = \frac{E^{\omega}_{22}}{3(1+s^2)^2}. \tag{68}$$

Displacement element. The conforming, exactly integrated isoparametric element DispPP is matched by setting

$$\begin{aligned} R_{11} &= \frac{1}{3}\left(E_{11}{+}4E_{13}s + (2E_{12}{+}4E_{33})s^2 + 4E_{23}s^3 + E_{22}s^4 + (E_{33}{+}2E_{23}s{+}E_{22}s^2)\gamma^2\right), \\ R_{12} &= \frac{1}{3\gamma}\left(E_{13} + (E_{12}{+}2E_{33})s + 3E_{23}s^2 + E_{22}s^3 + (E_{23}{+}E_{22}s)\gamma^2\right), \\ R_{22} &= \frac{1}{3\gamma^2}(E_{33} + 2E_{23}s + E_{22}(s^2{+}\gamma^2)). \end{aligned} \tag{69}$$

The StressPP element (as well as its clones Q6 and QM6) is again bending optimal along both x and y_ω (median) directions. The symbolic verification is far more involved than for the rectangular element because it requires the use of free-free flexibility methods[96] and is omitted.

A.1 Trapezoidal Panel

The geometry of the trapezoidal panel shown in Figure 18 is defined by the dimensions a, $b = a/\gamma$ and the two angles ω_1 and ω_2, both positive counterclockwise. Define

$$s_1 = \tan\omega_1, \quad s_2 = \tan\omega_2, \quad s = \tfrac{1}{2}(s_1+s_2), \quad d = \tfrac{1}{2}(s_1-s_2), \quad \phi = bd/a = d/\gamma. \tag{70}$$

The template is again given by the matrix form (31). Matrices $\mathbf{H}_c$ and $\mathbf{W}$ are as in (63), except that s has the new definition (70). The higher order projector matrix is

$$\mathbf{H}_h = \tfrac{1}{2}\begin{bmatrix} 1-\phi & 0 & -1+\phi & 0 & 1+\phi & 0 & -1-\phi & 0 \\ 0 & 1-\phi & 0 & -1+\phi & 0 & 1+\phi & 0 & -1-\phi \end{bmatrix}, \tag{71}$$

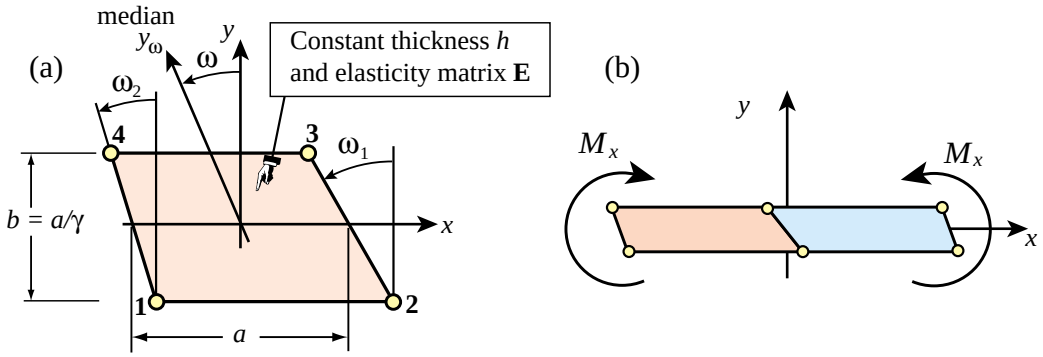

Figure 18. The four noded trapezoidal panel and a two-trapezoid repeatable macroelement.

whereas **R** depends on the formulation, as detailed next.

Stress element. Element StressTP is generated by the 5-parameter stress assumption (65), with one change: the (1,4) entry y/b is replaced by $(y - y_C)/b$. If $y_C = -b^2(s_2 - s_1)/(12a) = -\frac{1}{6}ad/\gamma^2$ the bending stresses are energy orthogonal to constant stress fields. The stiffness matrix derived with the HR principle is matched by

$$R_{11} = \frac{1}{C_{11}(3 - d^2/\gamma^2)}, \quad R_{12} = 0, \quad R_{22} = \frac{1}{3C_{22}^{\omega}(1 + d^2/\gamma^2)(1 + s^2)^2}, \tag{72}$$

in which C_{22}^{ω} is the compliance along the median y_ω (cf. Figure 18), given by (64).

QM6 element. The incompatible-mode element QM6[69] is no longer a clone of the stress element unless $d = 0$. Its stiffness is matched by

$$R_{11} = \frac{1}{C_{11}(3 - d^2/\gamma^2)}, \quad R_{12} = 0, \quad R_{22} = \frac{1}{C_{22}^{\omega}(3 - d^2/\gamma^2)(1 + s^2)^2}. \tag{73}$$

The only change is in R_{22}. The original incompatible-mode element Q6 of[68] fails the patch test if $d \neq 0$ and consequently cannot be matched by the template (31).

Strain element. Element StrainTP is generated by the 5-parameter strain assumption (67), with one change: the (1,4) entry y/b is replaced by $(y - y_C)/b$. Energy orthogonality is again obtained if $y_C = -b^2(s_2 - s_1)/(12a) = -\frac{1}{6}ad/\gamma^2$. A strain-fitting variational formulation[95] yields a stiffness matched by

$$R_{11} = \frac{E_{11}}{3 - d^2/\gamma^2}, \quad R_{12} = 0, \quad R_{22} = \frac{E_{22}^{\omega}}{3(1 + d^2/\gamma^2)(1 + s^2)^2}, \tag{74}$$

in which E_{22}^{ω} is the direct elasticity along the median y_ω direction, as given by (64).

Displacement element. The conforming isoparametric displacement element DispTP with 2×2 Gauss integration is matched by

$$\begin{aligned}
R_{11} &= \frac{E_{11} + 4E_{13}s + s^2(2E_{12} + 4E_{33} + 4E_{23}s + E_{22}s^2) + (E_{33} + 2E_{23}s + E_{22}s^2)\gamma^2}{3 - d^2/\gamma^2}, \\
R_{12} &= \frac{E_{13} + s(E_{12} + 2E_{33} + 3E_{23}s + E_{22}s^2) + (E_{23} + E_{22}s)\gamma^2}{\gamma(3 - d^2/\gamma^2)}, \\
R_{22} &= \frac{E_{33} + 2E_{23}s + E_{22}(s^2 + \gamma^2)}{\gamma^2(3 - d^2/\gamma^2)}
\end{aligned} \tag{75}$$

A.2 A Unidirectional-Bending-Optimal Trapezoidal Panel

Element StressTP is x-bending optimal as an individual element, but far from it as a repeating macroelement. Consider the configuration of Figure 18(b): two mirror-image trapezoidal elements are glued to form a parallelogram macroelement. The macroelement shape is that of a swept panel, and is obviously repeatable along x.

If $a >> b$ and $s_1 \neq s_2$ the StressTP-fabricated macroelement rapidly becomes overstiff and overflexible in x- and y-bending, respectively. For example if $a/b = \gamma = 8$, $s_1 = 0$, $s_2 = 1/2$ and isotropic material with $\nu = 1/4$ the bending ratios are $r_x = 11.97$ and $r_y = 0.1414$. For the anisotropic elasticity matrix (61), $r_x = 6.93$ and $r_y = 0.0792$. If an elongated macroelement is supposed to model unidirectional x-bending correctly, the overstiffness caused by $s_1 \neq s_2$ is called *distortion locking*. This phenomenon has been widely studied since the MacNeal-Harder test suite gained popularity.[97]

It is possible to construct a trapezoidal panel that is exact in unidirectional x bending when configured to form a repeatable macroelement as in Figure 18(b), for any aspect ratio γ as well as arbitrary side slopes s_1 and s_2. This template instance will be called UBOTP. A compact expression is obtained by taking the **R** matrix of StressTP, generated by (72) and modifying the (2,1) entry of **W**:

$$\mathbf{W} = \begin{bmatrix} 1/a & 0 \\ -\dfrac{\left(C_{11}(3\gamma^2 - ds) + C_{13}\right)(s-d) - C_{12}d}{C_{11}(3\gamma^2 - d^2)b} & 1/b \end{bmatrix} \tag{76}$$

It would be equally possible to keep **W** of (63) and adjust the entries of **R**. However, the correction (76) suggests how this optimality result is extendible to arbitrary quadrilaterals.[3] It is not difficult to prove that $\mathbf{W}^T\mathbf{R}\mathbf{W}$ for UBOTP is positive definite as long as the trapezoid is convex. [Not only that: its condition number is bounded, which is another way of saying that the inf-sup — also called LBB condition — is verified.] Consequently the element stiffness is nonnegative, and has the correct rank.

Figure 19 presents results for a widely used mesh distortion test, which involves one macroelement of the type discussed. Results for six element types: UBOTP, StressTP, StrainTP, DispTP, Q6 and QM6 are shown. The percentage of the correct answer is of course $100/r_x$.

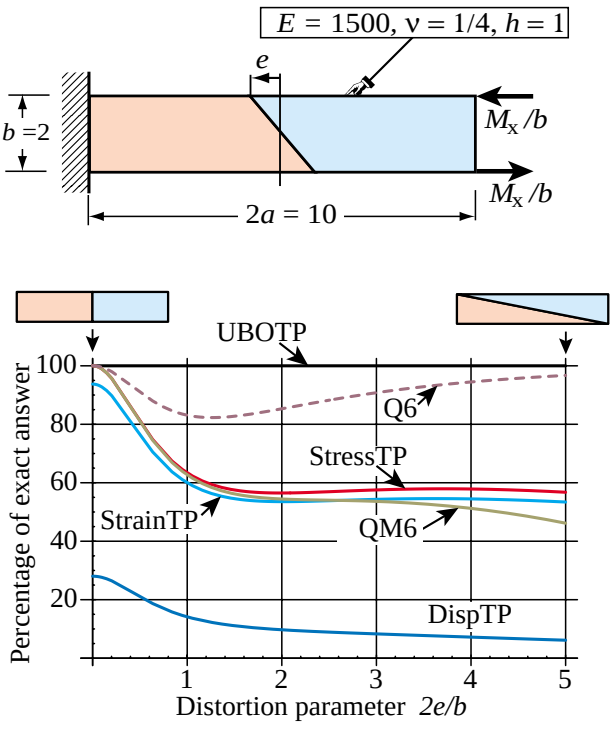

Figure 19. A well known distortion benchmark test. Dashed lines mark elements that fail the patch test (only Q6 in this particular set).

Of these six models only Q6 fails the patch test, but otherwise works better than all others but UBOTP. StressTP, StrainTP and QM6 give similar results, as can be expected, whereas DispTP is way overstiff even for zero distortion. UBOTP gives the correct result for all distortion parameters from 0 through 5, since $r_x \equiv 1$. If the aspect ratio of the

cantilever is changed to, say $2a/b = 10$, the differences between elements become more dramatic.

For distortion performance results on other elements such as Pian-Sumihara and Enhanced Assumed Strain, see Lautersztajn and Samuelsson.[72] A penalty-augmented modification of the Pian-Sumihara quadrilateral constructed by Wu and Cheung[98] that achieves distortion insensitivity at the cost of rank deficiency (and hence fails the inf-sup condition) is discussed in the sequel.[3]

At first sight the existence of UBOTP contradicts a theorem by MacNeal,[2] which says that four noded quadrilaterals cannot simultaneously pass the patch test and be insensitive to distortion. The escape hatch is that y-bending optimality (along the skew angular direction ω_1 of the macroelement) is not attempted. If one tries imposing $r_x = r_y = 1$, the solutions for $\{R_{11}, R_{12}, R_{22}\}$ become complex if $\gamma >> 1$ as soon as d deviates slightly from zero.